AD-A115 288 NATIONAL BUREAU OF STANDARDS WASHINGTON DC FRACTURE A--ETC F/G 11/2
EFFECT OF CONTACT DAMAGE ON THE STRENGTH OF CERAMIC MATERIALS.(U)
OCT 81 S M WIEDERHORN, B J HOCKEY, J S NADEAU N00014-81-F-0002

UNCLASSIFIED NL

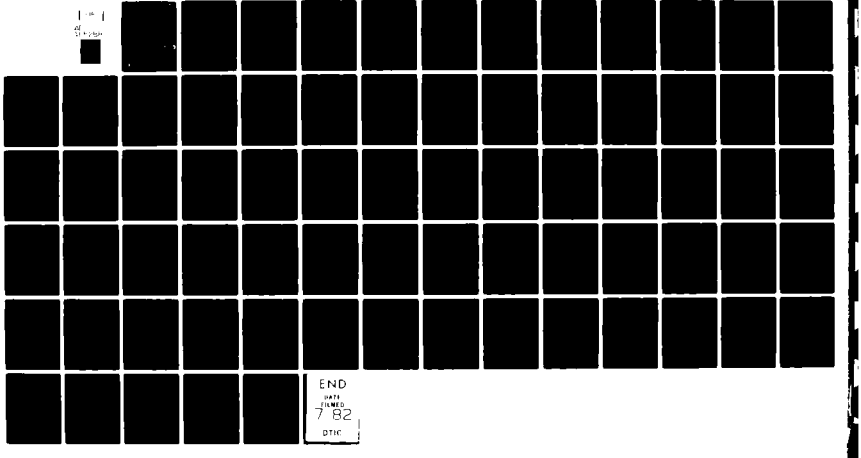

END
DATE FILMED
7 82
DTIC

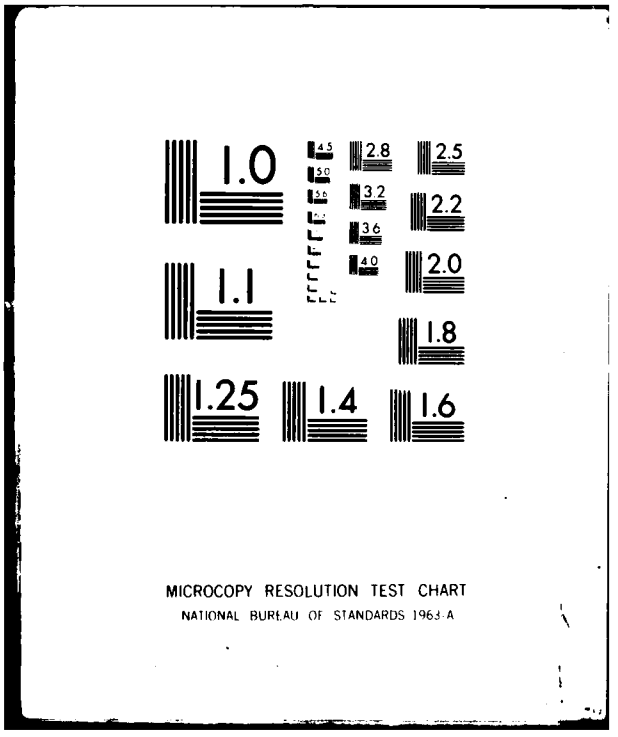
1.0
1.1
1.25
1.4
1.6
1.8
2.0
2.2
2.5
2.8
3.2
3.6
4.0
4.5
5.0
5.6
MICROCOPY RESOLUTION TEST CHART
NATIONAL BUREAU OF STANDARDS 1963-A

NR 032-607

Effect of Contact Damage on the Strength of Ceramic Materials

S. M. Wiederhorn, B. J. Hockey, and J. S. Nadeau

Technical Report

ONR Contract No. N00014-81-F-0002
NBS Project No. 5620453

for

Office of Naval Research
Arlington, VA 22217

by

National Bureau of Standards
Washington, DC 20234

October 1981

Effect of Contact Damage on the Strength of Ceramic Materials

S. M. Wiederhorn, B. J. Hockey, and J. S. Nadeau

Technical Report

ONR Contract No. N00014-81-F-0002
NBS Project No. 5620453

for

Office of Naval Research
Arlington, VA 22217

by

National Bureau of Standards
Washington, DC 20234

October 1981

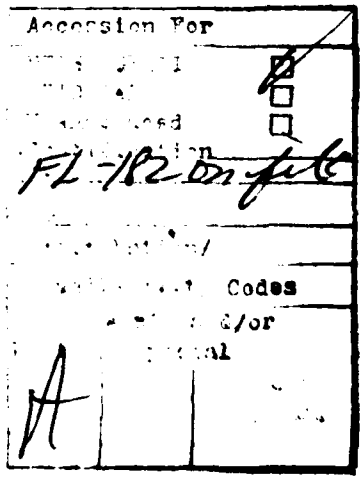

FOREWORD

This report describes the results of an experimental program to investigate mechanisms of contact damage in ceramic materials at elevated temperatures, and to determine the effect of this damage on the strength and wear of ceramic materials.

Table of Contents

EFFECT OF CONTACT DAMAGE ON THE STRENGTH OF CERAMIC MATERIALS

S. M. Wiederhorn
National Bureau of Standards
Washington, D.C. 20234

Abstract

The primary objective of this research is the development of a deeper understanding of the physical processes that result in contact damage between components of heat engines at elevated temperatures. Rates of mechanical junction formation will be measured, and the effect of these junctions on friction, crack formation, and strength degradation will be investigated. Major material parameters to be studied will include ceramic composition, microstructure, hardness, and fracture toughness. The data obtained will be used for the assessment of theoretical treatments of strength degradation caused by sliding contact stresses. During the past year, equipment has been constructed to measure the adhesive and frictional forces that develop between ceramics at elevated temperatures. Some tests have been conducted on glasses to determine the temperatures at which the friction is enhanced as a result of adhesion at the contact interface. Studies indicate that the coefficient of friction increases precipitously at a temperature that is ~ 200 °C below the fictive temperature, suggesting that at this temperature, glass is sufficiently mobile for junctions to form at the glass interface.

In addition to this work on adhesion and friction, studies conducted in previous years on the erosion of ceramics at elevated temperatures have been summarized. Erosion data are compared with two theories that have been suggested to explain the erosive behavior of solids. A dimensional analysis is applied to the variables that are important to erosion, and a

multivariant, linear regression analysis is used to fit the data to the dimensional analysis. The results of the linear regression analyses are compared with the two theories in order to evaluate the applicability of these theories to erosion. Although semi-quantitative agreement of the data with the theories is obtained, some discrepancies are apparent. In particular, the dependence of erosion rate on hardness and critical stress intensity factor is greater than predicted by either of the two theories. These discrepancies are attributed primarily to microstructural aspects of erosion that are not modeled by either of the theories.

EFFECT OF CONTACT DAMAGE ON THE STRENGTH OF CERAMIC MATERIALS

S. M. Wiederhorn
National Bureau of Standards
Washington, D.C. 20234

and

J. S. Nadeau
University of British Columbia
Vancouver, B.C.

1. Introduction

Stresses caused by the physical contact of ceramic components can result in severe localized surface fracture of these components. This type of damage occurs in many applications of structural ceramics and is particularly severe in heat engines. Relative motion of segmented sections of these engines during operation, combined with sizable loads and adhesion, results in the formation of cracks at contact sites between components. If the stresses in the component are large enough, these cracks propagate, resulting in component failure under normal operating conditions. This type of failure has been a major impediment to the success of the ceramic turbine engine program supported by the Advanced Research Projects Agency and monitored by the Department of the Navy [1].

Contact processes, such as those just described, are studied in the field of science known as tribology. Of general interest to investigators in this field are the magnitude of the forces and stresses that result from solid-solid contact, and the type and extent of damage that occurs during contact. The area of real contact between the two solids is of prime importance to the establishment of the magnitude of the stresses that develop during solid-solid contact.* When two solids are displaced by an external load, the force for

*Material properties that control adhesion and plastic deformation at the contact interface are also important, and are also to be considered in this project.

separation or relative motion depends on the real area of contact. Any chemical or physical process that increases the area of contact will enhance the force required for separation or motion. The real contact area is particularly important for high temperature applications where sintering and chemical reactions significantly increase the area of contact.

In this research project we focus our attention on the effect of high temperature and corrosive environment on the real area of contact between two surfaces and the effect of this area on the strength of materials. Past studies have suggested that surface reactivity at elevated temperatures is important in establishing the area of contact. Chemical reactions and liquid phase sintering at the contact site are particularly important in causing the area of contact to increase. Ceramics for heat engines, for example, are most often made of silicon nitride, or silicon carbide, both of which are glass formers at elevated temperatures (in oxidizing environments). As has been shown by Rabinowicz [2], Miller et al. [3], and Richerson et al [4], coefficients of friction increase by a factor of ten ($f \sim 0.2$ at ambient tmperature to $f \sim 3$ at 1200 °C) when oxide glasses form on ceramic surfaces. Enhancement of the friction coefficient occurs as a result of the increased area of contact due to glass formation. Since forces during sliding friction are proportional to the coefficient of friction, oxidation results in surface stresses at elevated temperatures that are an order of magnitude larger than those in the absence of surface oxides. These surface stresses can result in surface cracking and strength degradation that are detrimental to the operation of heat engines at elevated temperatures.

Surface oxidation causes more serious contact damage if sintering also occurs between two components. Then the components are no longer separated by a viscous interface, but are bonded into a monolithic structure. Relative

motion of the two components requires the material between the components to be ruptured, resulting in strength degradation because of crack formations at the junction. Because oxide coats contain the elements that are normally used for the hot-pressing of silicon nitride and silicon carbide at high temperature, sintering of these ceramics may be an important phenomenon limiting the lifetime of engine components. Studies have not been conducted to elucidate the role of contact sintering during high temperature engine operation, or the effect of such sintering on component reliabilty.

Contact damage caused by mutual sliding of components in heat engines has not been studied in depth, and appears to be a major limiting factor in the development of engines for both military and commercial operations. Areas of research that are needed to clarify our understanding of contact damage include mechanical junction formation during high temperature exposure and effects of these junctions on the stress distribution in components that are in contact. Data resulting from such investigations will serve as the basis for theoretical modeling of strength degradation and for predicting component reliability. Furthermore, once a basis of understanding of contact damage has been developed, means of avoiding such damage should be possible, either through mechanical design of surfaces of contact or through chemical alteration of surfaces of contact.

2. Theoretical Approach

The objective of this research project is the enhancement of our understanding of contact damage in structural ceramics. To achieve this objective the initial stages of our project will be divided into two principal parts: first, to study junction formation and adhesion that results from high temperature exposure; second, to investigate the effect of such junctions on the strength of the surfaces of contact. As a general guide to the research project, this section deals with several aspects of the contact problem.

2.1 Junction Formation and Adhesion at Elevated Temperatures

Materials scientists have studied junction formation extensively on both metals and ceramics to gain information on the initial stage of sintering. Initial stage sintering involves the formation of a "neck" between contacting particles, which are usually modeled as spheres. The main driving force for neck formation is the reduction of surface free energy that occurs as the interface between the particles disappears (figure 1)[5]. Material transport to neck region occurs because the chemical potential of material in the region of the neck is lower than that on the surface of the sphere. As can be seen from table 1, several alternate mechanisms for neck formation have been identified, the controlling mechanism is determined by the easiest transport path for a given solid. For each of these mechanisms, the neck size, x, has been evaluated as a function of time, t, particle size, r, temperature, T, surface energy, γ, and parameters that are related to the mechanism of transport. For example, the theoretical relation between these variables for lattice diffusion is given by the following expression:

$$x = (40\gamma\, a^3\, D^*/kT)^{1/5} r^{2/5} t^{1/5} \qquad (1)$$

where k is Boltzman's constant, a^3 is the atomic volume of a diffusion vacancy, and D^* is its diffusion coefficient. Similar expressions have been published for the other mechanisms of neck formation listed in table 1, and for neck formation in the presence of an active liquid [6].

Table 1. Alternate Paths for Matter Transport During the Initial Stages of Sintering [5]

Mechanism Number	Transport Path	Source of Matter	Sink of Matter
1	Surface diffusion	Surface	Neck
2	Lattice diffusion	Surface	Neck
3	Vapor transport	Surface	Neck
4	Boundary diffusion	Grain boundary	Neck
5	Lattice diffusion	Grain boundary	Neck
6	Lattice diffusion	Dislocations	Neck

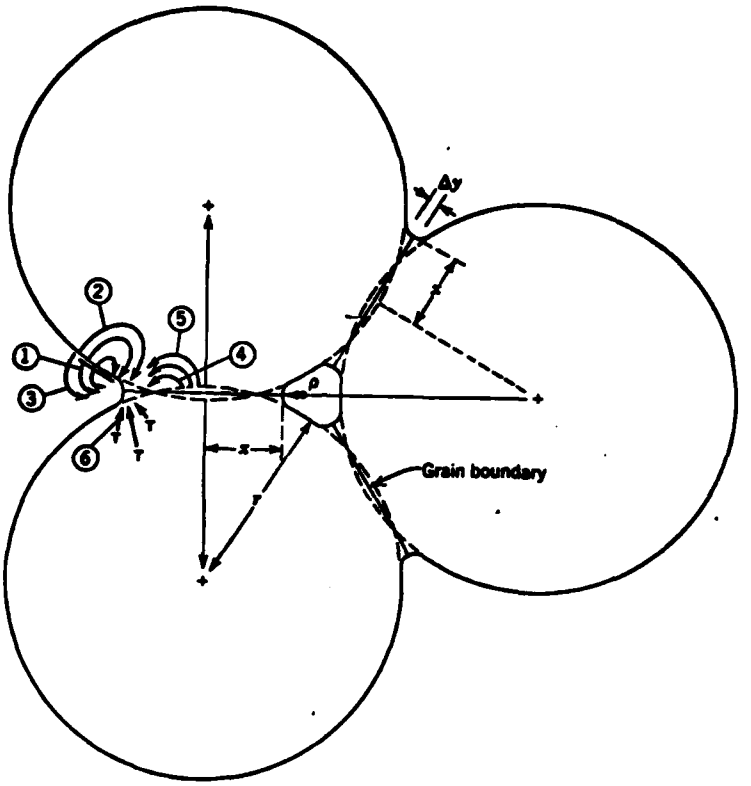

Figure 1. Alternative paths for materials transport during the initial stages of sintering [5].

With regard to adhesion of ceramic components, initial stage sintering theory may provide the basis for understanding the development of the real area of contact between ceramic components at elevated temperatures. If the temperatures are high enough, the surfaces will sinter together in a manner that is predicted by initial stage sintering theory, and the real area of contact between two surfaces will be determined by the size of the neck formed during sintering. Because of the dependence of neck size on parameters such as surface free energy, diffusivity, time, and surface curvature (Eq. 1), the real contact area will also depend on these parameters. The rate of sintering is expected to be sensitive to oxygen in the environment since silicon carbide

and silicon nitride are glass formers. It is anticipated that neck formation for these materials will be controlled by liquid phase sintering and will be effected by the rate of oxidation and the rate of formation of glass at the interface.

2.2 Shear Strength of Contact Junctions

Once the real area of contact between ceramic surfaces has been determined, the maximum shear force required to rupture the junction can be calculated by use of the theory of notches developed by Neuber [7]. For a deep external circumferential notch, which simulates the geometry of the contact surfaces, the maximum tensile strength on the surface of the notch is given by

$$\sigma = p\,[1 + 1/2\,(x/\rho^{1/2}] \qquad (2)$$

where ρ is the radius of curvature of the tip of the notch, x is one-half the width of the external notch, and p is the shear stress applied to the notch ($p = F/\pi x^2$, where F is the remotely applied shear force). The half width of the notch as described in Eq. (2) is identical to the neck radius, x, used in the sintering equation. The location of the maximum stress is determined in terms of the curvalinear coordinate system used to describe notches. Hence, both the shear strength of a contact junction and the location of the origin of the fracture can be predicted from the available literature on notches. If the sintering equation for neck size [Eq. (1)], is now substituted into the equation for the maximum tensile stress at the surface of a notch [Eq. (2)], it is possible to predict the shear strength (and therefore the coefficient of friction) of the junction as a function of the experimental parameters (time, temperature, sphere radius) discussed in 2.1 of this report.

Determination of the maximum shearing force for rupture solves only part of the problem arising from the sintering of ceramic components at elevated temperatures. Once the neck area is broken, mechanical damage is left on the surfaces of the ceramic components, and it is this damage that is the cause of strength degradation of these components. Hence, it is important to evaluate the type and extent of surface damage at broken junctions and to determine the effect of this damage on component strength. Unfortunately, the damage is not easily characterized theoretically because of the complexity of the stress field at the contact junction, and the lack of information on the crack path trajectory when the junction is broken.

3. Experimental Approach

With regard to our work on adhesion of non-oxide ceramics, the rate of neck formation in these materials will be studied. Experimental variables will be temperature, sphere radius, time, and oxygen partial pressure. Once the rate of formation of the contact radius has been determined, a quantitative theory of neck formation will be developed along the lines of that outlined in section 2 of this report. The rate of neck formation will be related to the strength of the bond formed between the two surfaces, the coefficient of friction of the material, and the type of damage that results from mechanical rupture of the neck.

In the initial stages of the program, the rate of neck growth will be evaluated using standard sintering techniques. Ceramic spheres will be placed on plates of the same material and will be annealed to varying lengths of time and temperature in vacuum, oxygen, and air. Since normal forces during sintering may play an important role in engine applications, experiments will be conducted with a load applied normal to the plate surface. The size of the neck will be determined after annealing by breaking the spheres loose

from the plate. Subsequent to characterizing the rate of neck growth for the experimental conditions noted above, a second set of experiments will be conducted using a more limited set of experimental conditions. In these experiments, the spheres will be separated from the plate by application of a force normal to the substrate. The force required for separation of the sphere from the substrate will be used as a measure of the strength of the bond formed during sintering. The broken junctions will be examined by scanning electron microscopy to characterize the microstructure of the sources of failure. The force for rupture of the sintered bond will be related to the size of the neck by using Neuber notch theory [7], in a manner similar to that to be discussed in the next section of this report.

Turbine materials to be studied will include reaction-bonded and hot-pressed silicon carbide and silicon nitride. In addition to these materials, a set of data will be obtained on glass and on high density aluminum oxide. The data on these materials will be used as examples of adhesive bond formation under circumstances for which chemically active sintering does not occur. Theoretical modeling of bond strength should be easier for these materials than for the non-oxide ceramics used in turbines. Data on the glass and aluminum oxide will be compared with that of the silicon nitride and silicon carbide to determine if the mechanisms of sintering and strength degradation are similar for these different types of materials.

To evaluate the nature and severity of damage at the contact site, experimental studies will be conducted to characterize the size of flaws formed when a contact junction is ruptured by a shear force. Therefore, we propose to measure the shear forces required to rupture junctions that have been formed by sintering. A high temperature friction apparatus has been constructed to accomplish this goal. The apparatus is capable of applying

both normal and tangential loads to a specimen surface at temperatures as high as 1500 °C. Based on the sintering studies, a sintered junction will be formed between a spherical slider and a flat substrate that will be in the form of a four-point bend specimen. The shear forces required to break the junction will then be measured and compared with theoretical predictions obtained from notch theory. After the bond is ruptured, the contact surface on the sphere and the four-point bend specimen will be examined microscopically to evaluate the type of damage that occurs during fracture. The four-point bend specimen will then be broken to evaluate its strength and to characterize the flaw origin that determines its strength. As in the sintering study, experimental variables will be time of exposure, temperature, and radius of the spherical slider. Following this procedure, it should be possible to characterize both the crack trajectory and the type of damage left behind on the contact surface. This information combined with information obtained on sintering rates should be useful in developing a complete theory on the strength of contact junctions, and the amount of strength degradation resulting from the fracture of these junctions.

4. Progress to Date

4.1 Equipment

The equipment constructed to investigate adhesion and friction between ceramic components at elevated temperatures is of three types: first, to study adhesion; second, to measure frictional forces that develop between flat plates; third, to measure frictional forces that develop between a spherical slider and a plate. All three are designed to operate at elevated temperatures. The equipment should enable us to obtain data that will test the theory discussed in part 3 of this report.

The adhesion equipment is designed to press a sphere against a flat plate at elevated temperatures, hold the sphere against the plate for a predetermined period, and then to withdraw the sphere to measure the load required to rupture the bond that develops between the sphere and the plate. The initial set of equipment, to be used in a study of glass adhesion, is made of 304 stainless steel and is designed to operate at temperatures as high as 1000 °C. A schematic design of the experimental setup is shown in figure 2. Metal collars (not shown in the figure) are used to hold both the sphere and the specimen in place. The sphere and the plate are mounted in the hot zone of a furnace that is capable of 1600 °C. In a second design of this equipment, silicon carbide parts will be used to achieve the full capability of the furnace. Both specimen and plate will be lightly sintered in place to maintain their position during the adhesion experiment. The stainless steel apparatus should be adequate for experiments on glass, and should yield considerable information on both the process and the capability of the experimental design. Although the equipment has been completed, no experimental studies have been conducted on it as yet.

The second piece of equipment, figure 3, was designed to press two flat plates against a third, so that the frictional force required to withdraw the central plate from the outer two can be measured. The normal forces are applied by using a small pneumatic bellows. The apparatus is mounted in the heat zone of a furnace which is attached to a universal testing machine. By moving the cross head of the machine at a constant rate of displacement, and gradually increasing the furnace temperature, the sliding coefficient of friction can be measured as a function of temperature. The static coefficient of friction can also be determined by permitting the equipment to soak at temperature before attempting to measure the coefficient of friction. The

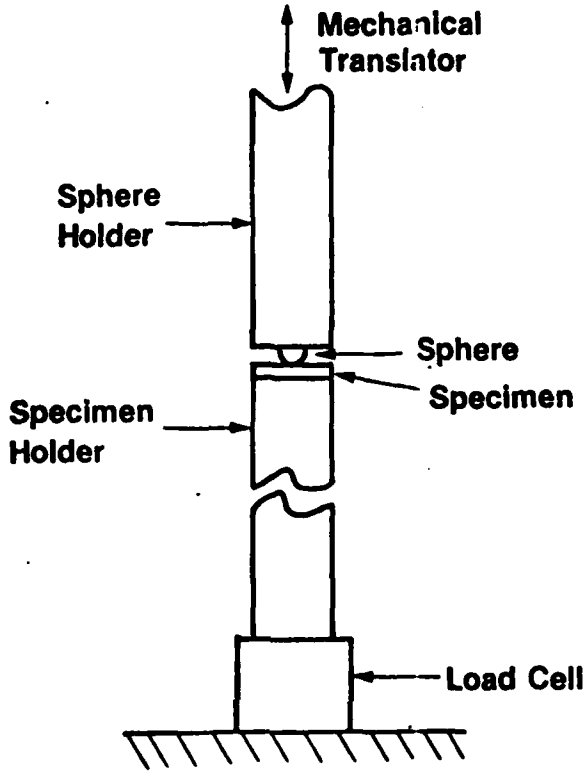

Figure 2. Schematic diagram of experimental apparatus to measure adhesion. Mechanical attachments for gripping the sphere and the specimen are not shown.

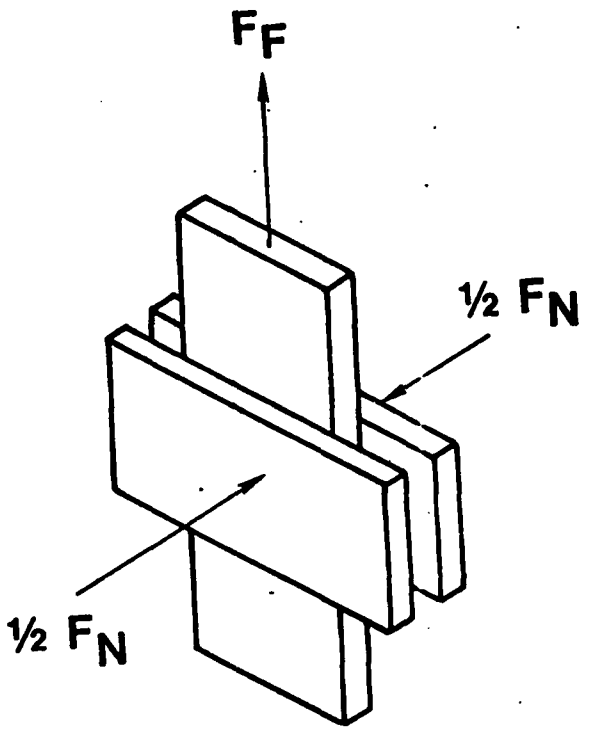

Figure 3. Schematic diagram used for studying the frictional behavior of flat plates. Equipment is constructed of stainless steel (304) and is suitable for studies to 1000 °C.

equipment is made of 304 stainless steel, and therefore only as a temperature capability of 1000 °C. However, this temperature should be sufficient for studies on glass and glass coated ceramics (i.e., oxidized Si_3N_4). Because of its complexity (not shown in figure 3), the equipment cannot be constructed of ceramic materials. If higher temperatures are necessary, a new set of equipment will be constructed of a high temperature alloy.

The third piece of equipment designed for high temperature studies of contact problems in ceramic materials is shown in figure 4. As can be seen from this figure, the equipment is designed to measure the frictional forces that develop when a sphere is pressed against a flat ceramic specimen. Both the normal and transverse loads are measured by the use of small load cells. The transverse load is applied by a hydraulic actuator which can translate the sphere approximately one-half inch during the course of the experiment so that both static and dynamic coefficients of friction can be measured. A hinge and ball joint is required for the normal load train to avoid the occurrence of spurious transverse forces during the course of the experiment. Since the ratio of the length of the normal load train to the distance transversed in the course of an experiment is in the ratio of 30 to 1, errors developed in the normal and lateral forces during the experiment are estimated to be less than three percent. The equipment is currently constructed of 304 stainless steel to evaluate its performance. However, the design is simple and silicon carbide load trains will be substituted for the stainless steel when high temperatures are necessary. The present equipment will be used at temperatures up to 1000 °C to evaluate the frictional behavior of glass, and the type of surface damage that develops as a result of such friction.

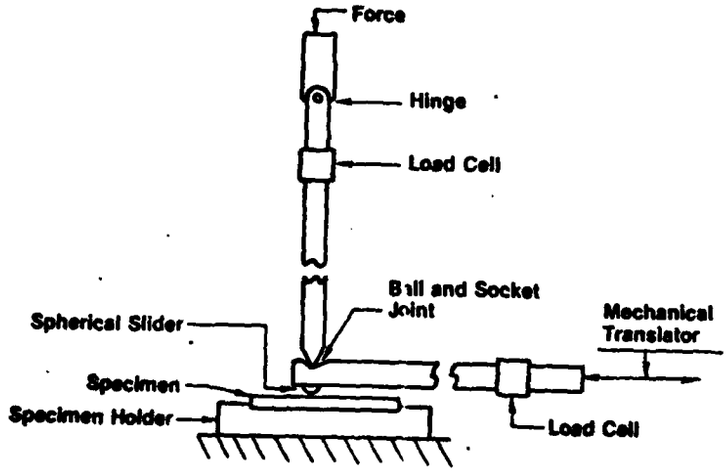

Figure 4. Schematic diagram of apparatus used to measure the frictional forces developed between a sphere and a flat plate. When constructed of silicon carbide, equipment will be capable of measurement to 1500 °C.

4.2 Experiments

Of the three sets of equipment designed for adhesion and wear studies, only the equipment for flat plate measurements was finished in time to obtain preliminary data on the sliding friction of glass at elevated temperatures. Some data were also collected on the equipment designed to measure sliding friction of sphere on plate, but they are too cursory to include in this report. The data do indicate, however, that the equipment works according to design. Friction studies on plates were conducted on three types of glass: soda-lime-silica glass; silica glass; high lead-silica glass (70 percent lead). These glasses were selected because they exhibit a wide range of annealing temperatures, which can be used as a measure of the refractoriness of the glasses. The lead glass and the soda-lime-silica glass had annealing temperatures of 417 °C and 520 °C, respectively, whereas the silica glass has an annealing temperature of 1050 °C.

Initial studies were conducted to determine the effect of normal force and surface finish on the sliding coefficient of friction. For most experimental studies of the friction of solids these parameters have been shown to have little effect on the coefficient of sliding friction. In the present investigation, the normal load was also shown to have little measurable effect on the coefficient of friction. For the range of loads covered, 10 N to 160 N, the coefficient of friction was relatively unchanged by the load, figure 5. Because of this observation, it was possible to restrict our studies to a single normal load, N, with some assurance that the data obtained would be representative of data obtained over a wide range of loads.

In contrast to our observation of the effect of load on coefficient of friction, surface roughness has a considerable effect on the coefficient of sliding friction, figure 5. The coefficient of friction of glass slides that

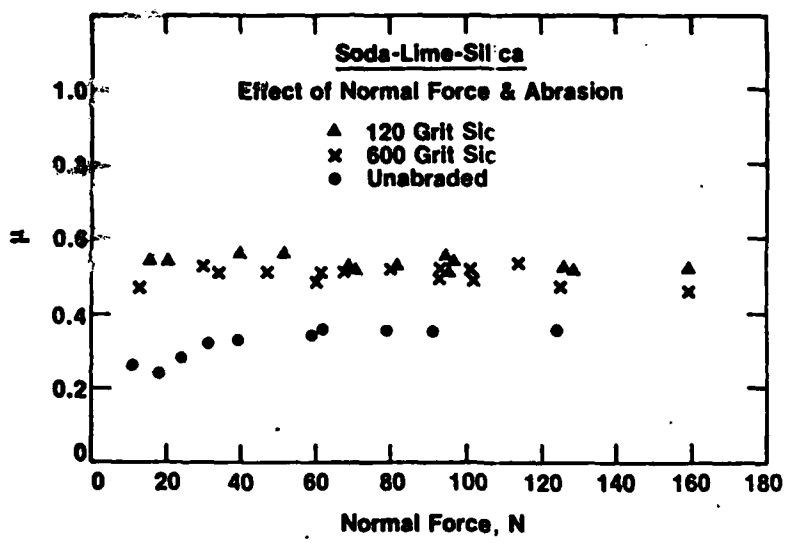

Figure 5. Effect of normal force and mechanical treatment of surface on the coefficient of friction of soda-lime-silica glass plates sliding against one another.

had been abraded was approximately 0.53, whereas the coefficient of friction of the unabraded glass was approximataely 0.35. The severity of abrasion, however, appeared to have little effect on the friction measurement, since the slides abraded with either the 120 grit abrasive paper, or the 600 grit paper gave friction results that were essentially undistinguishable. The difference in abrasion results suggests a difference in sliding mechanism for the two surface preparations. While an analysis of the sliding mechanism will have to await a detailed microscopic examination of the wear surfaces, a preliminary examination suggests that in the case of smooth surfaces, sliding is controlled by adhesion and plastic deformation at the surfaces of contact. The higher coefficient of friction of the abraded surfaces, however, may be the result of mechanical interlocking of one surface with the other, or gauging and abrasion by the asperities of the abraded surface. Alternatively, minor contamination of the unabraded surfaces may result in boundary lubrication which would lower the friction coefficient perceptibly. The true cause of the difference in friction behavior for the two surface treatments will have to await further investigation.

The friction results taken at elevated temperatures are shown in figures 6 to 8 for the soda-lime-silica glass, the lead glass, and the silica glass, respectively. The most apparent difference between the three sets of curves is the sharp rise that occurs at about 400 °C in the friction coefficient for both the lead glass and the soda-lime-silica glass, but not for the silica glass. This rise in friction coefficient occurs at about 200 °C below the annealing temperature of these two glasses, and is probably the result of a considerable increase in the real area of contact between the two sliding surfaces as the temperature approaches the annealing temperature. The increase in contact area combined with the fact that glass is still quite resistant to

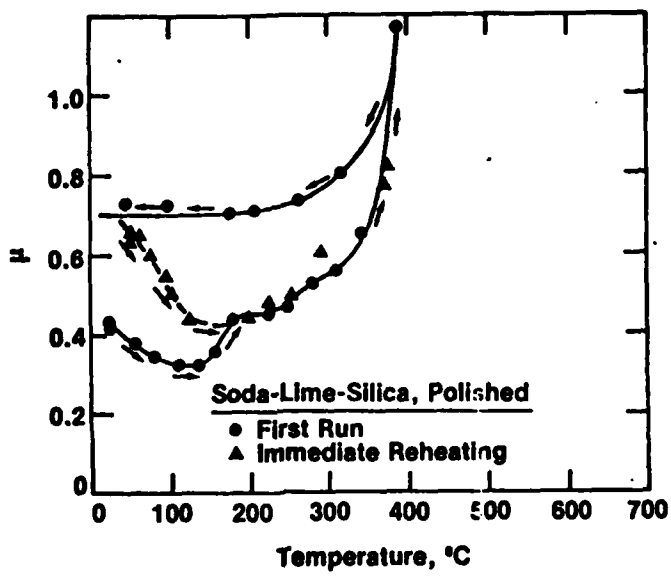

Figure 6. Effect of temperature on the coefficient of friction of soda-lime-silica glass plates.

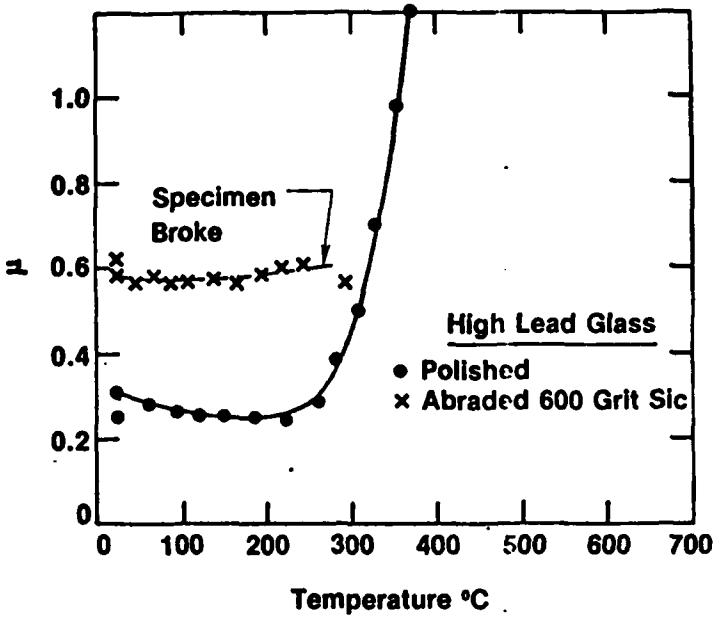

Figure 7. Effect of temperature on the coefficient of friction of lead glass plates.

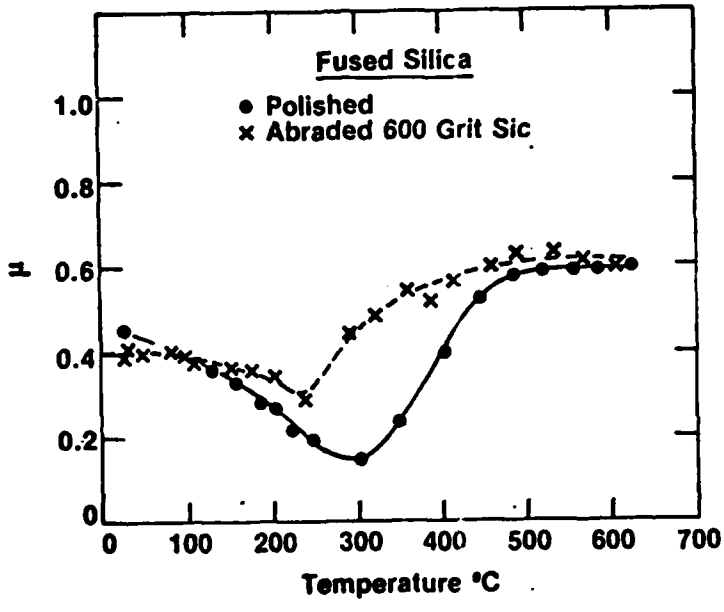

Figure 8. Effect of temperature on the coefficient of friction of silica glass plates.

plastic deformation in this temperature range would account for the rapid increase in friction coefficient. The absence of a rise in the friction coefficient of silica glass supports this conclusion since the annealing temperature of the silica glass is much higher than that of the other two glasses, and adhesion between silica glass surfaces is not expected to occur until very much higher temperatures are reached. Rabinowicz and Imai [2] in a study of the friction of glass forming ceramics have made similar observations.

The results just described have important ramifications with regard to frictional forces that develop between parts in heat engnes. The results suggest that the composition of glass that forms at the interface will be instrumental in controlling the magnitude of the friction coefficient, and hence, the forces that develop at the interface during sliding. The composition of glass that forms on a ceramic surface during oxidation is expected to be dependent on the composition of the refractory. Thus, magnesia-doped, hot pressed silicon nitride develops a magnesia glass at the surface, whereas reaction bonded silicon nitride develops a silica glass at the surface. Because magnesia glasses have a lower annealing temperature than silica glass, the peak frictional load for sliding contact between glass coated ceramics is expected to be different for the two glasses, the maximum occurring at a lower temperature for the magnesia glass. For purposes of engine design, it may be possible to dope the surface of the ceramics to control the composition of glass that develops at the surface. By engineering the surface composition of the ceramic, the temperature range for maximum surface friction can be adjusted so that the maximum frictional effects are not concommitant with the maximum normal forces developed between ceramic components during engine

operation. If this approach to surface control proves practical, it should be possible to reduce the surface forces that result in component failure during the critical range of engine operation.*

A second feature of the friction data (figures 6 to 8) that is of interest, is the decrease in friction coefficient that occurs at low temperatures for the soda-lime-silica glass and the silica glass. Although it is tempting to attribute this effect to a surface contamination and desorption process (perhaps caused by water in the environment), this explanation is probably not valid for two reasons: (1) the effect is not observed in the lead glass; (2) the effect is observed in the soda-lime-silica glass when a second run immediately follows the first run. Hence, we must conclude that the decrease in friction coefficient and the hysteresis shown in figure 6 are not understood at the present time.

The effects of surface roughness on the coefficient of friction observed for the soda-lime-silica glass at room temperature, are also observed for the lead glass as a function of temperature. For the temperature range 25 °C to 300 °C, the coefficient of friction of specimens abraded with 600 grit abrasive paper is found to be twice that obtained for the unabraded glass surface. With regard to surface roughness, the silica glass behaves somewhat differently than the other two glasses. Effects of roughness on the friction coefficient were observed to develop as the temperature increased from room temperature, and completely disappeared at temperatures greater than 500 °C. Within the temperature range (~ 150 °C to ~ 500 °C) where surface roughness is important,

*One possible cause of failures in engines that use reaction bonded silicon nitride is the concurrence of the maximum frictional stresses and the maximum engine stresses during periods of peak power output.

specimens with abraded surfaces exhibit a much higher coefficient of friction than do the unabraded specimens. The reasons for these observations are not yet understood.

5. Research Plans

During the coming year work on friction and strength degradation of glass will be continued. Glass is not only an ideal model material for study because of its optical clarity, but is also of practical importance because it coats silicon nitride and silicon carbide at elevated temperatures. Measurements will be made on the rate of mechanical junction formation in glass at temperatures that lie below the glass transition temperature. The effect of normal load on the rate of junction formation will be investigated. Once the rate of junction formation has been characterized, the effect of these mechanical junctions on static friction, crack formation, and strength will be determined. Friction and strength data obtained on both sets of high temperature friction equipment (one to measure friction between plates, the other to measure friction between spheres and plates) will be correlated. The data obtained on this program will be compared with the predictions of the theory presented in section 2 of this report. A period of approximately one year will be required to complete this phase of the program. Once this work on glass has been completed other ceramics will be studied. Of particular interest will be glass forming ceramics such as silicon nitride and silicon carbide. The effect of surface glass on junction formation, friction, and strength will be determined. The program will parallel the one on glass and the data obtained in the two studies will be compared. In addition to these studies, some studies will also be conducted on aluminum oxide. Data on aluminum oxide will be of interest to separate frictional effects due to

glass from effects due to the uncoated substrate. The experimental procedure followed for the aluminum oxide will be essentially identical to that followed in other parts of the program.

6. References

[1] Ceramic Gas Turbine Engine Demonstration Program, Interim Report No. 15, Airesearch Report No. 76-212188 (15), Nov. 1979, Airesearch Manufacturing Co. of Arizona, P. O. Box 5217, Phoenix, Arizona 95010.

[2] E. Rabinowicz and M. M. Imai, "Boric Oxide as a High Temperture Lubricant," Paper No. 61-LUBS-17, Lubrication Symposium, Miami, Florida, May 8-9, 1961, Am. Soc. Mech. Engrs.

[3] D. G. Miller, C. A. Anderson, S. C. Singhal, F. F. Lange, E. S. Diaz, and R. Kossowsky, Brittle Materials Design, High Temperature Gas Turbine Material Technology, Vol. VI, Army Materials and Mechanics Research Center Report No. AMMRC CTR 76-32, December, 1976.

[4] D. W. Richerson, W. D. Carruthers, and L. J. Lindberg, "Contact Series and Coefficient of Friction Effects on Ceramic Interfaces," pp. 661-676, in Surfaces and Interfaces in Ceramic and Ceramic-Metal Systems, Materials Science Research, Vol. 14, Joseph Pask and Anthony Evans, eds., Plenum Press, New York (1980).

[5] W. D. Kingery, H. K. Bowen, and D. R. Uhlmann, Introduction to Ceramics, John Wiley and Sons, New York (1976).

[6] W. D. Kingery, J. Appl. Phys., 30, 301 (1959).

[7] H. Neuber, Theory of Notch Stresses, Springer Publishers, Berlin (1958), NTIS No. AECTR-4547.

[8] F. F. Lange and B. I. Davis, "Development of Surface Stresses During the Oxidation of Several Si_3N_4/CeO_2 Alloys," J. Am. Ceram. Soc., to be published.

[9] M. H. Lewis and B. S. B. Harunaratne, "Determination of High Temperature K_I-v Data for Si-Al-O-N Ceramics," pp. 13-32 in Fracture Mechanics Methods for Ceramics, Rocks, and Concrete, S. W. Freiman and E. R. Fuller, eds., ASTM STP 745, American Society for Testing and Materials (1981).

Figure Captions

1. Alternative paths for materials transport during the initial stages of sintering [5].

2. Schematic diagram of experimental apparatus to measure adhesion. Mechanical attachments for gripping the sphere and the specimen are not shown.

3. Schematic diagram used for studying the frictional behavior of flat plates. Equipment is constructed of stainless steel (304) and is suitable for studies to 1000 °C.

4. Schematic diagram of apparatus used to measure the frictional forces developed between a sphere and a flat plate. When constructed of silicon carbide, equipment will be capable of measurement to 1500 °C.

5. Effect of normal force and mechanical treatment of surface on the coefficient of friction of soda-lime-silica glass plates sliding against one another.

6. Effect of temperature on the coefficient of friction of soda-lime-silica glass plates.

7. Effect of temperature on the coefficient of friction of lead glass plates.

8. Effect of temperature on the coefficient of friction of silica glass plates.

Effect of Material Parameters on the Erosion Resistance of Brittle Materials

S. M. Wiederhorn and B. J. Hockey
National Bureau of Standards
Washington, DC 20234

1. Introduction

Erosion mechanisms for brittle materials are currently viewed as involving elastic-plastic impact events in which material is lost from the target surface by brittle fracture[1,2]. Nevertheless, the impact of a particle with a hard surface is known to result in the formation of a plastic zone at the impact site[3-5]. Residual stresses associated with this plastic zone force small cracks, known as lateral cracks, to grow from the impact site. Initially these cracks grow parallel to the target surface, but then curve toward and eventually intersect with the surface resulting in the loss of material from the target.

A significant body of experimental data is consistent with the above elastic-plastic interpretation of brittle material erosion. Microscopic studies of the surface of brittle solids that have either been eroded by many particles or impacted with single particles reveal residual impressions that are similar to Knoop or Vickers hardness indentations. Because of this similarity in appearance, early interpretations attributed these impressions to plastic deformation which occurs in the same way as in ductile metals. Subsequently, transmission electron microscopy was used to show unequivocally that these impressions are due to plastic deformation at the impact site[3-5]. Regardless of the material studied (Si, Ge, Al_2O_3, SiC), dense tangles of dislocations are found beneath the immediate area of impact[6]. The occurrence of plastic deformation at the impact site, and the observation that cracks formed at the impact site appear to be similar regardless of material, suggests a common mechanism of erosion for brittle materials.

As a result of the above studies on the microstructure of impact sites, two elastic-plastic theories have been developed to explain the brittle erosion of solids. Both are based on the assumption that lateral cracks grow in a quasi-static manner as a result of residual plastic stresses introduced by the impact event. In both theories, the size of the lateral cracks, c, are assumed to be determined by the Roesler relation[7]*

$$P/c^{3/2} = \beta K_c \qquad (1)$$

where P is the maximum normal load during impact, K_c is the critical stress intensity factor, and β is a nondimensional constant. The volume of material removed during erosion, V, is determined from the size of the lateral crack, c, and the depth of the crack, d, beneath the target surface

$$V = \pi c^2 d \ . \qquad (2)$$

Since the impact sites are assumed to be noninteracting, the total wear volume, W, is just the summation of the volumes resulting from the individual impact events.

The two elastic-plastic wear theories differ in their assumed dependence of impact load, P, on the kinetic and material parameters that are important to erosion. The theory developed by Evans et al.[8] includes dynamic stress wave effects in the calculation of P. A spherical particle is assumed to penetrate into a target without distortion; the contact pressure is assumed to be equal to the dynamic pressure that occurs when the particle first hits the target surface. The depth of penetration is determined from the time of

*The Roesler relation is concerned with the formation of radial cracks from an indentation. For the relation to be valid, the crack must be large relative to the size of the indentation. The use of this relation to describe lateral crack formation is based on work by Evans et al.[8] who showed experimentally that the size of the two cracks were proportional. Hence, the use of Eq. (1) to describe erosion phenomenon has its basis in empirical investigations and has no theoretical justification.

contact and the mean interface velocity, both of which are calculated from a one-dimensional analog. The final expression for the erosion rate, W, developed by Evans et al. is

$$W \alpha v_o^{3.2} R^{3.7} \rho^{1.6} K_c^{-1.3} H^{-0.25}[(Z_t Z_p)^{2/3}/(Z_t^{1/2}+Z_p^{1/2})^{8/3}] \qquad (3)$$

where Z_t and Z_p are the impedances for the target and the particle, respectively. The term within the brackets varies by less than 10 percent for the materials used in the current study, and therefore will be considered to be a constant for the purposes of this paper. Hence, the equation for the erosion rate obtained by Evans et al. reduces to

$$W \alpha v_o^{3.2} R^{3.7} \rho^{1.6} K_c^{-1.3} H^{-0.25} \qquad (4)$$

A quasi-static formulation of the erosion problem is based on work by Wiederhorn and Lawn[9], in which the kinetic energy of the particle is assumed to be absorbed completely by plastic flow when a particle impacts the surface. From this assumption, both the maximum force during contact and the maximum depth of penetration can be calculated. Assuming that the lateral cracks generate at a distance beneath the surface that is equal to the maximum depth of particle penetration, the following equation for the erosion rate is derived[2]

$$W \alpha v_o^{2.4} R^{3.7} \rho^{1.2} K_c^{-1.3} H^{0.11} \qquad (5)$$

The forms of the two erosion theories presented above are similar in that they express the erosion process by a power law dependence of erosion rate on both particle (v_o, R, ρ) and target (K_c, H) properties. Although the same properties are used in both theories, the power exponents for velocity, particle density, and hardness differ. A comparison of these theories with experimental results on erosion indicates that the theories are reasonably consistent with experiment with regard to the exponents for velocity and particle size[2]. The effect of particle density on erosion has not been investigated in any systematic manner, so that there is no way to know if the

exponents given in Eqs. (4) and (5) are correct. A study of the effect of hardness, H, and fracture toughness, K_c, on erosion has recently been conducted on a series of ceramics by Evans et al.[8] and by Gulden[10]. The data obtained by Evans et al. suggest a greater dependence of erosion rate on K_c and H than is predicted by their theory. Aside from these studies, however, there have been no systematic investigations of the effect of K_c and H on the erosion rate of brittle materials.

In this paper the erosion of dense brittle materials is studied to assess the validity of the erosion theories represented by Eqs. (4) and (5). Of particular interest to this study are the particle velocity and the material parameters K_c and H. The results of our study will show that while both theories provide a qualitative description of the erosion data, neither theory is quantitatively correct. The reason for these differences seems to lie in the simplifying assumptions made in both theories of erosion. As will become apparent, details of the microstructure and material interaction during impact affect erosion in ways not fully accounted for by the present models of erosion.

2. Experimental Procedure

The target materials used in the present investigation provided a reasonably wide range of target properties (K_c and H) and microstructure for study (table 1). Examination of the impact area by transmission electron microscopy showed that all of the materials selected for investigation deformed plastically when subjected to impact[6*]. The cracks that were generated by the impacting particles, while originating from within the deformed zone, exhibited no evidence for

*The technique of transmission electron microscopy was applied only to the crystalline materials used in this investigation. With regard to their deformation and fracture properties, however, other studies suggest the behavior of glass is similar to the crystalline materials (see reference 6 for a discussion of this point).

localized plastic deformation at the crack tip, and accordingly propagated in a brittle manner. Therefore, these materials fit within the framework of the theories discussed above.

The particles used for erosion measurements were 150 μm SiC abrasive grains. Because of the hardness of these particles it was felt that they simulated the hard, non-yielding particles assumed to be responsible for erosion in the theories used to derive Eqs. (4) and (5). To achieve a uniform particle size for investigation, all particles were sieved between an 80 and 120 mesh screen before using them for investigations of erosion. The particles that were used passed through the 80 mesh screen, but were retained by the 120 mesh screen.

The erosion apparatus used in this study has been described previously[11]. Briefly, the equipment was designed to feed abrasive particles into a high velocity airstream, which projected the particles against the specimen surface, figure 1. The particles were accelerated by passing them through a tungsten carbide nozzle ∿ 2 in. long and 1/16 in. in internal diameter. The acceleration of the particles to high velocity is accomplished within the nozzle. The particle-air mixture is passed through a ceramic tube 3/4 in. in diameter to obtain a relatively uniform beam of abrasive particles. High temperatures can be achieved in the equipment by feeding a propane-oxygen mixture through a ring-burner into the top of the ceramic tube. The high velocity particle-air stream sucks the flame from the burner into the 3/4 in. tube to produce temperatures as high as 1200 °C.

The particle velocities were measured by using a time-of-flight technique developed originally by Ruff and Ives[12]. In this technique, two disks rotate on a common axis which is parallel to the direction of the erosive gas stream. The disk closest to the exit port of the erosion apparatus has a slit in it.

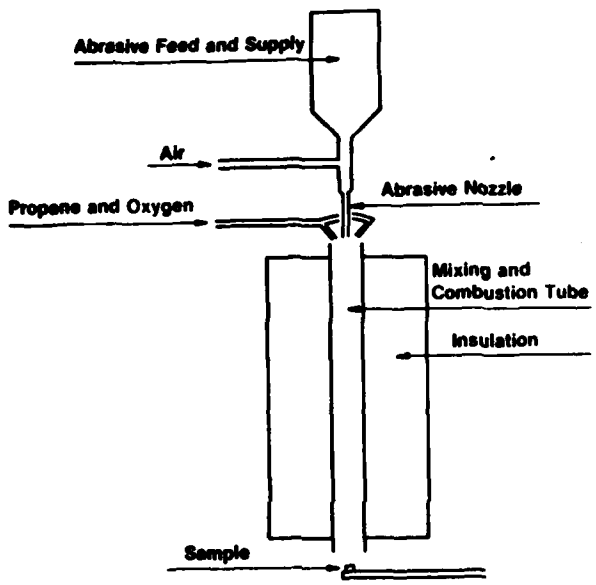

Figure 1. Schematic diagram of erosion equipment (after Wiederhorn and Roberts [11]).

The slit permits particles to pass through it and impinge on the second disk. For a fixed rotational speed, the position of the erosion mark on the solid disk, relative to the position of the slit on the first disk, establishes the particle velocity.

The sensitivity of the double disk technique to measure particle velocities was improved during the course of the present study by mounting partially silvered glass microscope slides on the solid disk directly below the slit on the first disk[13]. Particles that impinged on the glass slide formed impact damage that destroyed the reflectivity of the microscopy slide in the immediate area of impact. As a consequence, the position of the erosion marks on the microscope slides were more easily observed and measured. Quantitative optical microscopy was used to improve the accuracy of measuring the position of the erosion marks on the microscope slides. The original technique was further improved by first rotating the disk in one direction to obtain an erosion mark and then in the opposite direction to obtain a second erosion mark. This procedure doubled the distance between marks, thus improving the accuracy of the velocity measurements.

The specimens used in this study were 1/2 in. square plates approximately 1/4 in. thick. They were mounted on a support arm and held with their wide face normal to the stream of erosive particles. Specimens were exposed to a fixed mass of erosion particles, which ranged from 25 g to 400 g depending on the target material and the particle velocity selected for study. The mass lost by the target during each experiment was measured to at least one percent accuracy using an analytical balance. The erosion rate was calculated from the fraction of particles that intersected the specimen. The number of particles impacting the target was estimated from the mass of abrasive used and the mean particle size of the abrasive (approximating the particles as

spheres). Finally, the volume loss per particle impact (i.e., the erosion rate) was estimated from the mass lost from the specimen per particle impact, and the target density.

3. Experimental Results

The results of our erosion studies are shown in figures 2 to 4*. Figure 2 presents the results obtained at room temperature. The erosion rate, expressed in terms of volume lost per particle impact, was measured for velocities ranging from 37 m/s to 94 m/s, for the nine target materials used in the present study. The erosion data shown in figure 2 fit a power law function as expressed by Eqs. (4) and (5). The slope of the curves at room temperature ranged from 1.9 for hot-pressed silicon carbide to 2.9 for silicon and silica glass. The standard error of the slopes ranged from $\sim$ 0.003 to $\sim$ 0.25 with a mean value of $\sim$ 0.1 (table 2), which indicates that at the 95 percent level and for two degrees of freedom, a difference in slope of $\sim$ 0.4 is significant. With the exception of the hot-pressed silicon nitride, the values of these slopes are similar to those reported by other investigators on similar materials[14-19]. The slope of the hot-pressed silicon nitride was about one-half that reported earlier by Gulden[10]. The erosion rate of the target materials shown in figure 2 decreases as the toughness of the target material increases, a finding that provides qualitative support for the erosion theories described by Eqs. (4) and (5). A quantitative comparison of the two theories with the data will be made in a later section of this paper.

The erosive wear data collected at 500 °C and 1000 °C are shown in figures 3 and 4, respectively, for several of the target materials used in the present study. The data shown in these figures are similar to those obtained at room temperature. However, for certain materials the slopes of the curves

*The data used in these figures are summarized in Appendix B.

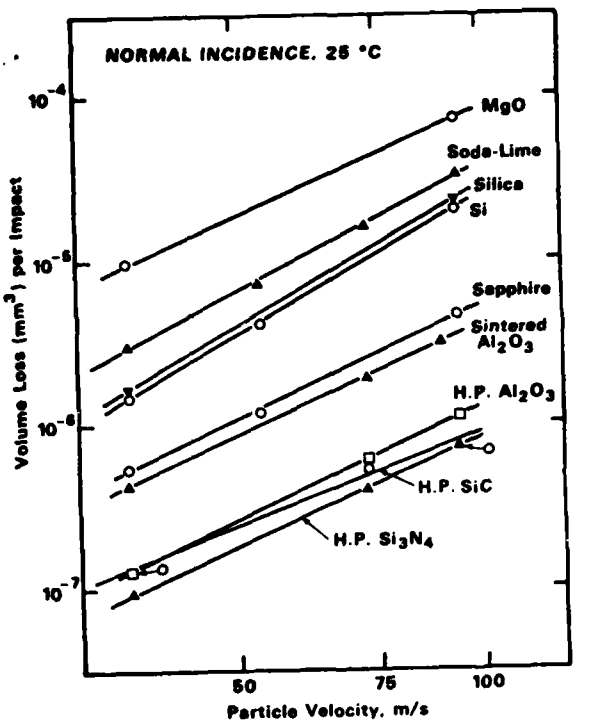

Figure 2. Erosion of brittle materials at 25 °C, normal incidence impact, 150 μm SiC particles. For clarity, the error bars given in Table 1A have been left off the figure.

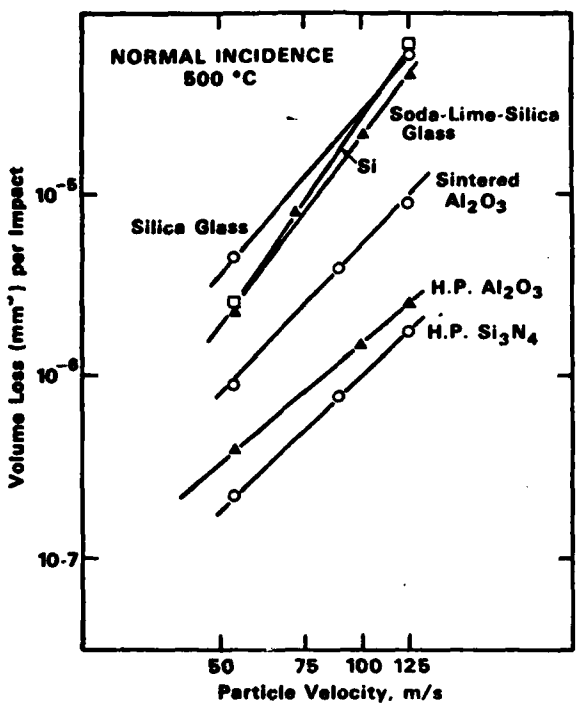

Figure 3. Erosion of brittle materials at 500 °C, normal incidence impact, 150 μm SiC particles. For clarity, the error bars of table 1A have been left off the figure.

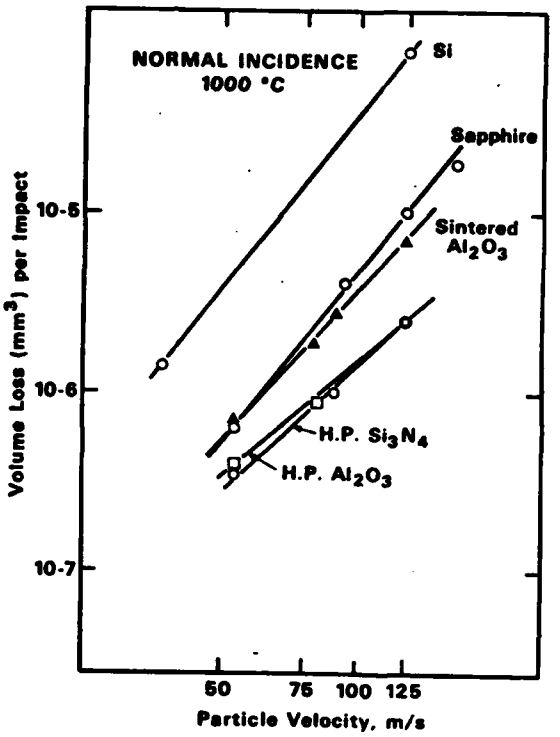

Figure 4. Erosion of brittle materials at 1000 °C, normal incidence impact, 150 μm SiC particles. For clarity, the error bars of table 1A have been left off the figure.

at elevated temperatures were significantly greater than those obtained at room temperature. Although the relative position of the erosion curves on the graph was roughly the same at elevated temperature and room temperature, small systematic differences in erosion behavior were obtained for each material. Thus, elevated temperatures appeared to slightly enhance the erosion rate of hot-pressed silicon nitride and hot-pressed aluminum oxide at the highest velocities, whereas the erosion rate of glass and sintered aluminum oxide was reduced at elevated temperatures most notably at the lowest velocities. The results of the present study were similar to those reported earlier by the present authors on a smaller set of data[4].

4. Discussion of Results

The purpose of this paper is to present data that can be compared with the elastic-plastic theories [Eqs. (4) and (5)] that have been developed to explain the erosion of brittle materials. The exponents of Eqs. (4) and (5) that can be compared with the present set of data are the velocity exponents and the exponents for K_c and H. Since K_c and H are determined by the target material and its microstructure, they cannot be varied independently, and hence have to be compared with the theories represented by Eqs. (4) and (5) in combined form, for example, $K_c^{-1.3}H^{-0.25}$ for Eq. (4), or $K_c^{-1.3}H^{0.11}$ for Eq. (5). A second way of comparing the exponents of Eqs. (4) and (5) with the experimental data is by first expressing these two equations in dimensionless form through the use of a dimensional analysis and then by fitting the dimensionless equation to the experimental data to obtain the exponents. Both of these techniques will be used in this paper.

4.1 Velocity Exponents

The velocity exponents obtained in this paper are summarized in table 2, and can be compared with other data reported in the literature for similar

materials, table 3. As can be seen from this table, data obtained in the present study are reasonably consistent with those reported by other authors. Most of the differences between the results shown in tables 2 and 3 are believed due to small, systematic, interlaboratory differences in experimental technique. The results on hot-pressed silicon nitride, however, seem to differ significantly from our own because of the large difference in velocity exponent (4 vs 2.2) obtained in the two studies.

A superficial comparison of the velocity exponents determined experimentally with those predicted from Eqs. (4) and (5) indicates that the exponents tend to cluster more closely about the value (2.4) predicted by the quasi-static model of erosion than the value (3.2) predicted by the dynamic model of erosion. This conclusion has to be tempered somewhat by the fact that the velocity exponent of v increases as the temperature is increased and tends to fall somewhere between the two predicted values. Furthermore, recent studies on silicon by Scattergood and Routbort[17] who investigated the dependence of velocity exponent on erosion-particle size suggests that the velocity exponent increases as the particle size decreases. Hence, for small particles, the trend is toward better agreement between the dynamic theory of erosion and experimental measurement. These reported dependences of velocity exponent on temperature and on particle size are not predicted by either theory, and in a sense, are a failing of both theories.

4.2 Target Parameters

The erosion data presented in figure 2 are compared with the material parameters H and K_c in figure 5. Figure 5a compares the erosion data with the dynamic theory of erosion, whereas figure 5b compares the erosion data with the quasi-static theory of erosion. With the exception of MgO, the data on both figures plot as straight lines, lending credence to the suggested

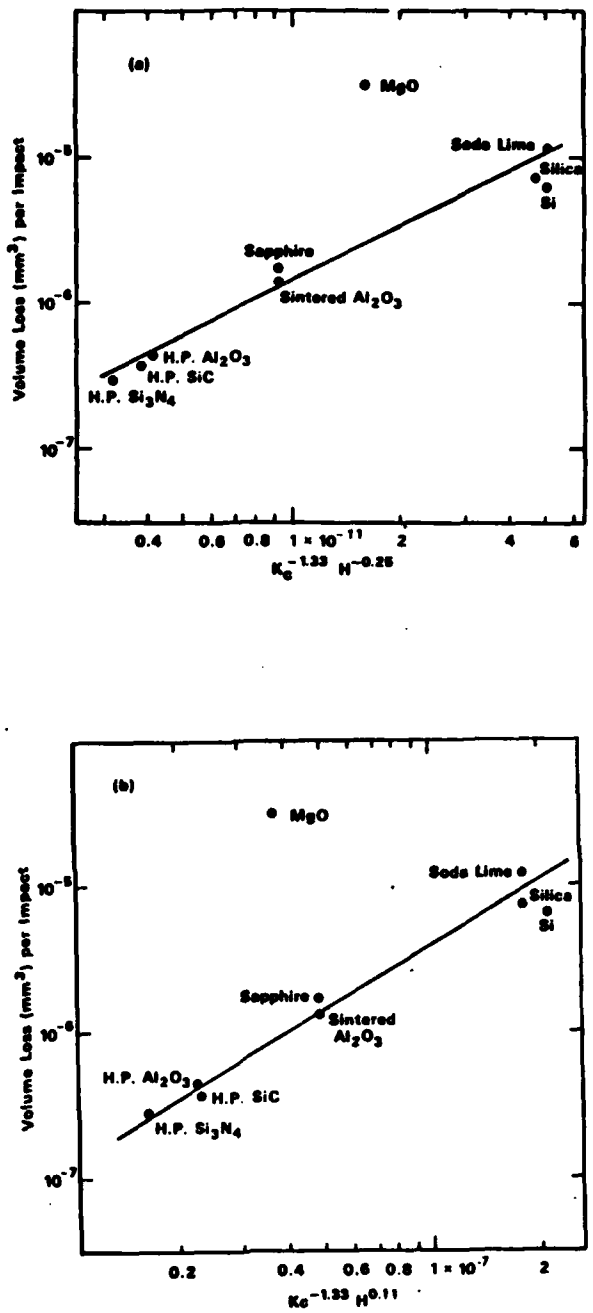

Figure 5. Comparison of the erosion data with the theories given by (a) Eq. (4)[8] and (b) Eq. (5)[2]. The volume lost per particle impact was selected from figure 2 at a velocity of 63 m/s. Units of hardness and toughness used to calculate the abscissae of this figure were Pa and Pa - $m^{\frac{1}{2}}$, respectively.

theories of erosion. However, both sets of data are represented by lines with slopes greater than 1, the theoretically expected slope. The empirical slope for the dynamic erosion theory, ~ 1.2, is closer to the expected slope of 1 than is the slope, ~ 1.5, for the quasi-static theory of erosion. Similar values of slopes were observed by Gulden[10] in an erosion study on a different set of materials. Hence, from this type of analysis, the dynamic theory of erosion appears to provide a somewhat better fit to the erosion data than does the quasi-static theory.

The type of plot given in figure 5a was used by Evans et al.[8] to test the validity of the dynamic erosion theory. The materials studied by these authors were MgF_2, reaction-bonded Si_3N_4, Al_2O_3, and hot-pressed Si_3N_4. The slope that they obtained, ~ 2, was considerably greater than the value 1.2, obtained from figure 5a. Furthermore, the data for the hot-pressed silicon nitride fell about one order of magnitude below the predicted curve. As noted recently by Gulden[10] the reason for this discrepancy between theory and experiment rests in the fact that quartz particles were used for the erosion tests. Quartz particles tend to break up on impact with hard surfaces (Al_2O_3, hot-pressed Si_3N_4) and hence remove less material during each impact event. The silicon carbide particles used in the present experiment and in the experiment by Gulden[10] are much harder and tougher than the quartz particles used by Evans et al.[8] and break-up upon impact is expected to be minimal. Furthermore, the silicon carbide particles are expected to penetrate most of the target materials in a manner predicted by the theory. We believe these explanations account for the fact that Gulden's data and our own data provide better support for the dynamic impact theory of erosion than did the original data presented by Evans et al.[8] in their discussion of the subject.

The data for MgO are not at all consistent with the data obtained for the other materials, undoubtedly because of the type of impact damage formed in the surface of this material. The MgO tended to crack along the grain boundaries in the vicinity of the impact site, so that each impact event formed a loosely connected aggregate of grains that surrounded the impact site. These damaged areas were easily removed from the surface during erosion, and therefore, their removal resulted in a higher rate of erosion than predicted theoretically. In essence, the mechanism of erosion for the MgO differed markedly from that for the other materials.

4.3 Dimensional Analysis

From the above discussion of the experimental data, we see that the theories that have been derived to explain the erosion of brittle materials are only partially successful in their description of the data. The quasi-static theory appears to be more consistent with the dependence of the erosion rate on velocity, whereas the dynamic theory appears to be more consistent with the dependence of erosion on materials parameters. The discrepancies undoubtedly arise from the complicated nature of the erosion process and the various simplifying assumptions that are used to obtain a model of erosion. Dimensional analysis[20] is an alternative method of obtaining relationships between the various parameters that effect erosion. While not providing a specific model of erosion, dimensional analysis provides an operative equation to describe erosion in terms of dimensionless groups and empirical constants determined from fits of experimental data. The empirical constants can be compared with those from the two erosion models to yield an unbiased comparison of theory and experimental data.

In analyzing the erosion process, we assume that the critical parameters that control erosion are those given in Eqs. (4) and (5). The volume loss per

particle impact, W, is then considered to be a function of these parameters

$$W = F\ (v_o,\ R,\ \rho,\ K_c,\ H) \qquad (6)$$

Using the standard methods of dimenional analysis[20], the following functional relation is obtained for the parameters given in Eq. (6):

$$W/R^3 = A(K_c^2/RH^2)^a\ (\rho\ v^2/H)^b \qquad (7)$$

where A is a dimensionless constant.*

Because Young's modulus has been suggested as a variable that contributes to crack formation during hardness indentations[21], the treatment given above was extended to include Young's modulus, E. The equation obtained is similar to Eq. (8), but contains an extra dimensionless term, E/H

$$W/R^3 = A'\ (K_c^2/RH^2)^a\ (\rho\ v^2/H)^b\ (E/H)^c \qquad (8)$$

Equation (7) contains three dimensionless groups each of which has physical meaning. The first represents the ratio of the volume loss during impact to the volume of the impacting particle. All other parameters being constant, the erosion rate will increase as the particle volume (i.e., particle size) increases. The second group (K_c^2/RH^2) can be represented as the ratio of the inverse of target brittleness to the size of the impacting particle. This interpretation follows from the fact that $(K_c/H)^2$ is a measure of the relative resistance of a target to fracture during an impact event: the higher the value of $(K_c/H)^2$, the more resistant the target will be to fracture. The parameter $(K_c/H)^2$ can be thought of as representing a critical scaling dimension above which fracture occurs during contact. In this sense, the inverse quantity, $(H/K_c)^2$, is a useful index of "brittleness."[21] The third group, $(\rho v^2/H)$ represents the ratio of the particle energy density, i.e., kinetic energy per particle volume, ρv^2, to the hardness, which can be considered as a deformation energy density. The fourth dimensionless constant in Eq. (8) can be considered as the ratio of the elastic to the plastic energy density.

*This equation is derived in Appendix A.

The constants a and b for the dynamic model of erosion, have values of -0.67 and 1.58, respectively. For the quasi-static erosion model, the values of a and b are -0.67 and 1.22, respectively. The value of c in Eq. (8) is zero for both models. Hence, the two models differ only in the exponent of the third dimensionless group. Since the two models differ in the assumed dependence of impact load on particle velocity, this difference in the exponent of the third dimensionless constant is not surprising.

Empirical values of the constants, a, b, and c for Eqs. (7) and (8) were obtained by a multiple regression analysis of the data reported in figure 2. The results of the analysis are given in table 4. The statistics in this table give useful information on the relative importance of the constants a, b, and c with regard to the fit of the erosion data. Virtually the same values of a and b and their standard errors are obtained regardless of whether two or three independent variables are used for the regression analysis. The standard errors for a and b are relatively small (7 and 11 percent of the mean, respectively) and the values of t computed for these constants are large and hence significant for any reasonable level of probability. By contrast, the standard error for c (55 percent of the mean) is large, and the value of t obtained for this constant is not significant at the 95 percent level, which suggests that the value of c reported in table 4 does not differ significantly from zero. From this discussion we conclude from our results that the wear rate does not depend in any significant way on the ratio of the Young's modulus to the hardness, E/H.* This conclusion is supported by the fact that r-squared, which gives the fraction of the variance accounted for by the regression analysis, only changes from 94 to 95 percent when E/H is added as

*This conclusion must be tempered by the fact that E/H only varied by a factor of ~ 2 in the present study. A larger variation of this parameter might indicate a significant dependence of wear on E/H.

an independent variable. Consequently, the values of a and b determined from the two parameter regression analysis will be used for purposes of further discussion in this paper.

As can be seen from table 4, the empirical value for a, -0.932, is greater in absolute value than the theoretical value of a, -0.667, given by Eqs. (4) and (5). The value for b, 1.38, lies approximately half-way between the value of 1.22 predicted by the quasi-static theory and the value of 1.58 predicted by the dynamic theory. Using the values of a and b from the multiple regression analysis, Eq. (8) can be expressed in a form that is similar to that of Eqs. (4) and (5)

$$W \alpha v^{2.8} R^{3.9} \rho^{1.4} K_c^{-1.9} H^{0.48} \qquad (9)$$

The most significant difference between Eqs. (4) and (5) and Eq. (9) is the dependence of the wear rate on the fracture toughness and the hardness. The exponent of K_c suggests a stronger dependence on this value than is predicted theoretically. As K_c of the target is increased, the difficulty of removing material by chipping increases more rapidly than predicted by either of the theoretical treatments of brittle erosion discussed in this paper. A possible source of this variation theory has to do with the effect of microstructure on erosion and the statistical nature in which the particles impact on the target surface. These sources of variation imply that the models suggested to explain erosion may be too simple to fully account for the effect of fracture toughness on the erosion rate. The effect of microstructure and the statistical nature of particle impact will be discussed more fully in a later section of this paper.

In view of the fact that most theories of erosion predict a decrease in the erosion rate as the hardness is increased, the positive exponent of the hardness in Eq. (9) requires some discussion and rationalization. In most

theories of erosion, hardness enters as part of a term that controls the depth of penetration during impact. Penetration of the impacting particle into the target surface is greater for soft materials. For ductile materials, the increase in penetration permits more material to be scooped from the target surface by the particle during erosion and therefore increases the size of the erosion fragments formed during each impact event. Although particle penetration is undoubtedly important to the erosion process in brittle materials, the positive exponent for hardness in Eq. (9) implies that hardness also enters the erosion process in another way so as to compensate for the negative exponent of H that results from the penetration components.

A clue to the positive exponent obtained for hardness in Eq. (9) can be obtained by a closer examination of the quasi-static theory of erosion. In this theory, hardness is used in two steps of the derivation. Hardness determines both the depth of penetration and the maximum load during impact. In the expression for maximum load, hardness enters the equations with a positive exponent, such that for a fixed depth of penetration the maximum impact load increases as the hardness is increased. Since the amount of chipping is proportional to the maximum load during impact, the relation between load and hardness suggests that the erosion rate will increase as the hardness increases. Penetration is also important to erosion because it determines the depth beneath the surface where lateral cracks form: the deeper the penetration (lower hardness) the greater the erosion rate. In the final equation for erosion, the penetration term and the load term oppose one another with regard to hardness. In the quasi-static model of erosion, Eq. (5), the penetration term is dominated by load term, and the net effect is a positive exponent for the hardness. Using this same line of reasoning, the results of the regression analysis suggest that hardness effects surface load

to a greater extent than it effects penetration depth, resulting in a positive exponent for hardness in Eq. (9). The fact that the exponent in Eq. (9) is greater than 0.11 suggests that the effect of the surface load term on erosion is greater than that predicted by the quasi-static theory of erosion.

4.4 Microstructural Analysis of Impact Damage

As noted in the previous section of this paper, the larger than predicted exponent of K_c in Eq. (9) may have its origin either in microstructural aspects of the erosion process or in the statistical nature of the way in which particles impact on the target surface. The two theories of erosion discussed in this paper are predicated on the assumption that the particles impact on sharp corners and that the type of damage formed is similar regardless of the properties of the target material. If either of these assumptions are not valid, then the observed erosion dependence on K_c would be expected to differ from that given by Eqs. (4) and (5).

Examination of the microstructure of surfaces that have been eroded by small numbers of particles yields information on both the type of damage that occurs during erosion and the relative number of particles that result in chipping from the target surface. When particles impact the target, they either leave shallow, plastic impressions, or small chipped regions at the point of impact, figure 6. The plastic impressions are left by particles that were probably oriented in such a manner that the impact was not on a sharp corner, but rather on a blunt side, or edge. The fact that plastic impressions were left on the target suggests that whereas the impact force was sufficient to cause deformation, the deformation was not concentrated sufficiently to nucleate and propagate cracks that would result in removal of material from the target. In other words, stresses at the impact site did not exceed the threshold for fracture at these shallow impressions. Consequently, only a

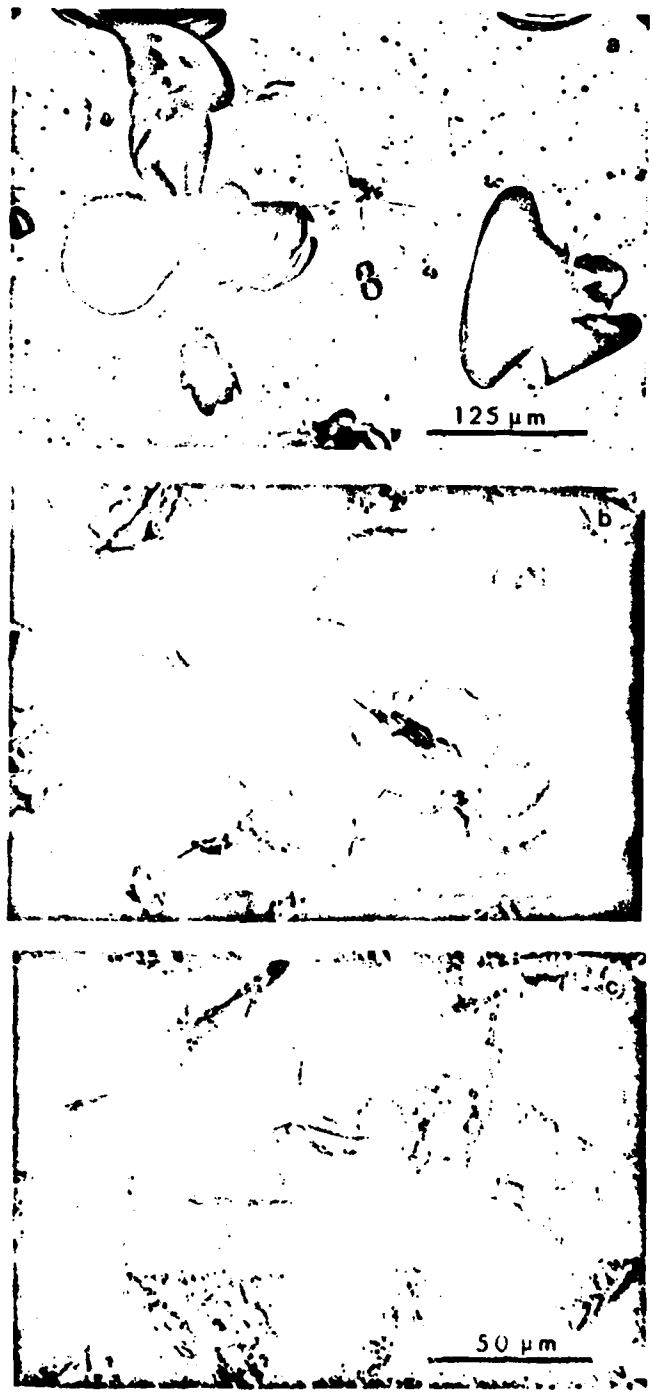

Figure 6. Single particle impact damage in ceramic materials, optical micrographs: (a) soda-lime-silica glass, 90 m/s; (b) sapphire, 90 m/s; (c) hot-pressed silicon nitride, 90 m/s.

fraction of particles that impact the target surface are effective in the removal of material. If this fraction depends on K_c, then the erosion of the target will also depend on K_c, but in a way not given by Eqs. (4) and (5).

In our study of the morphology of eroded surfaces we have observed that as the toughness of the material is increased, the relative number of impacts that result in chipping is greatly reduced, regardless of impact velocity. This observation of impact behavior is illustrated in figure 6, where erosion surfaces of glass, sapphire, and silicon nitride are compared. As can be seen, the fraction of impacts that results in fracture and material removal increases as the fracture toughness of the target decreases. For glass, every impact site in figure 6a has resulted in crack formation. By contrast, both the sapphire and the silicon nitride have several impact sites where plastic impressions were left, but where crack formation was not apparent. This observation suggests that the functional dependence of erosion rate on K_c for brittle materials is not completely described by either theoretical treatment of erosion (Eqs. (4) and (5)), but instead depends on factors that are related to the nucleation of cracks at the impact site. Apparently crack nucleation is relatively easier when a "blunt" impact occurs in glass or silicon, than when it occurs in the hot-pressed materials used in the present study. Hence, the rather large dependence of erosion rate on K_c and H reported in this paper can be attributed in part to statistical effects of particle orientation during erosion.

A second possible explanation for the observation of a larger than expected dependence of erosion rate on K_c and H has to do with the geometry of the cracks that form during the erosion process. The theories that have been proposed to explain erosion assume that cracks propagate from the impact site in a self-similar fashion. Once cracks are nucleated they are assumed to propagate

to the target surface so that material is removed from the target by each impact. In contrast to these expectations, microscopic examination of the target surface indicates that the effectiveness of material removal from the target seems to depend on the fracture toughness of the target. Thus for the hot-pressed materials used in this study, cracks are often observed to arrest within the solid, figure 7b and 7c, so that cracking during impact does not result in material loss from the target surface. A second or third impact in the vicinity of the primary impact site is needed for material to be removed from the target. In contrast to this behavior, complete chipping from the primary impact site is a more frequent occurrence for the more brittle materials such as silicon or glass, figure 7a. Thus, as the fracture toughness of the material increases, the efficiency of material removal per impact event is less than predicted theoretically, and the effect of K_c on the erosion rate is greater than predicted theoretically.

A more complete understanding of microstructural effects, particle orientation, and material response will have to await further theoretical modeling of the erosion process. It is worth noting, however, that the effects of a more accurate modeling on the erosion rate will probably not be large, as can be seen from the fact that the theories that have been proposed to explain erosion account for most of the dependence of erosion rate on the target parameters H and K_c. Theoretical refinement will, however, be necessary for a more complete understanding of the erosion process in brittle materials.

Before turning from the subject of microstructure it is worth commenting on the erosion results obtained for aluminum oxide and sapphire. As can be seen from figure 2, the erosion rates of sapphire and sintered aluminum oxide are approximately three times that of the hot-pressed aluminum oxide. The difference in behavior of the two polycrystalline materials is attributable

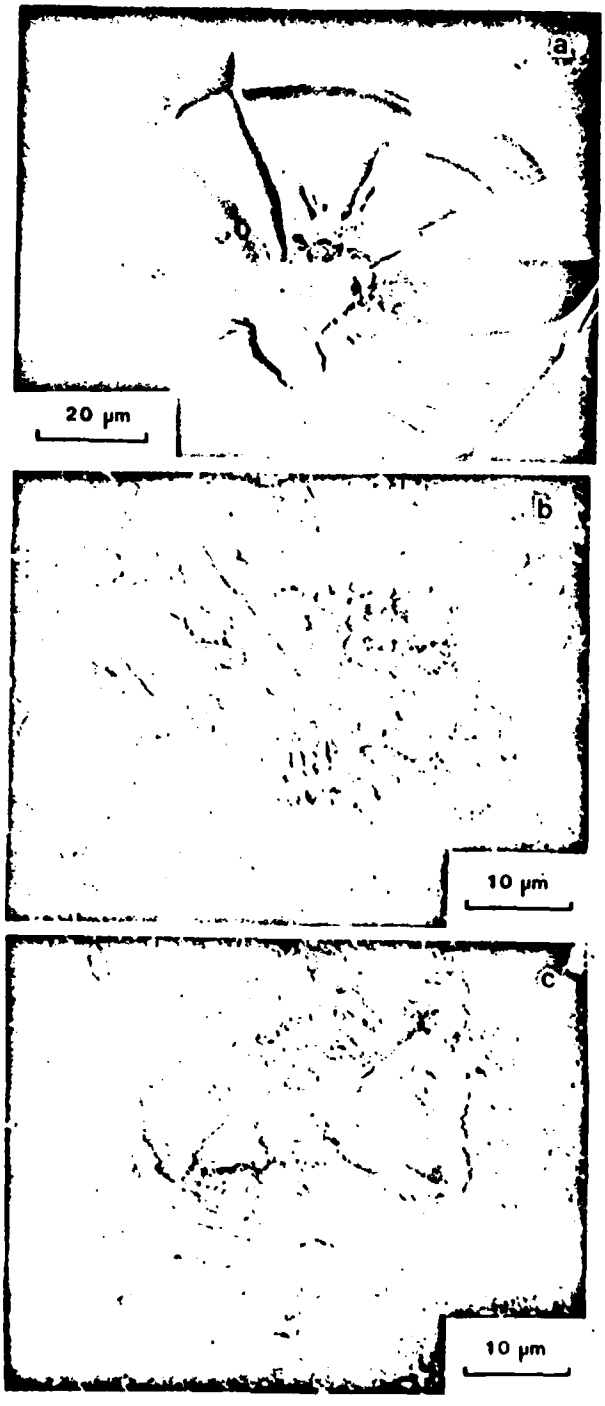

Figure 7. Single particle impact damage in ceramic materials, scanning electron micrograph: (a) soda-lime-silica glass, 54 m/s; (b) hot-pressed aluminum-oxide, 90 m/s; (c) hot-pressed silicon nitride, 90 m/s.

to the difference in grain size of the two materials. The grain size, 3-4 μm, of the hot-pressed material was considerably smaller than the size of the lateral cracks that were formed in this material upon impact. As a consequence, lateral cracks interact with many grains during propagation, and the effective value of K_c resisting the growth of lateral cracks is that typical of polycrystalline aluminum oxide, ~ 4 $MPa^{-m^{1/2}}$. By contrast, lateral cracks formed in the sintered aluminum oxide, grain size ~ 30 μm, are usually contained within a single grain, and the effective K_c resisting crack growth is more typical of values obtained from single crystal fracture measurements, ~ 2 $MPa^{-m^{1/2}}$. Using Eq. (9), the erosion rate for the large grain aluminum oxide should be approximately 3.7 times that obtained for the fine grained aluminum oxide. In figure 4, the erosion rate for the sintered aluminum oxide is approximately 3.3 times that of the hot-pressed material, which is close to the expected value. The fact that the erosion rate of the sintered aluminum oxide is close to that obtained for sapphire lends further support for this interpretation of the data.

4.5. Erosion at Elevated Temperatures

As can be seen by comparing figures 3 and 4 with figure 2, the temperatures employed in the present study appear to have a marginal effect on the rate of erosion. This finding is consistent with that reported earlier by the authors from a more limited set of data collected on some of the same materials studied in this paper[4]. Since dislocation mobility is enhanced by increasing the temperature, it was expected that both the hardness and fracture toughness, and hence the erosion rate, would be modified by increasing the temperature. Indeed, it has been shown that when loads are applied slowly, both the hardness and toughness of ceramic materials are strongly dependent on temperature[22-26]. The fact that significant changes in the erosion behavior are not observed

at elevated temperatures suggests that for conditions of dynamic loading, both the hardness and the toughness are invariant with temperature. This supposition is supported by dynamic toughness measurements on hot-pressed silicon nitride[27,28], and by the fact that cracks are observed to form in soda-lime-silica glass at temperatures above the softening point of this glass[29,30].

Although plastic flow does not play a dominant role in the erosion of ceramics under the conditions used in the present paper, minor differences between low and elevated temperature behavior can be attributed to plastic flow in some circumstances. Because lateral cracks form after the impact event and are driven by residual stresses at the impact site, relaxation of those stresses or modification of the resistance of the target to crack growth as a result of plastic deformation can alter the size of chips that are formed after the impact process. Such effects are feasible when the relaxation time of the material for plastic flow is shorter than the time required for the lateral cracks to complete their growth. In an earlier study on soda-lime-silica glass at 500 °C, the temperature dependence of the erosion rate was, in fact, attributed to such plastic relaxation[29]. In the present study, the small differences between low and elevated temperature behavior may be attributable to the same types of processes. For example, changes in the mode of crack propagation from trans-granular at room temperature to inter-granular at high temperatures for the hot-pressed aluminum oxide and silicon nitride suggests a decrease in the resistance of the grain boundaries to fracture. Despite the possibility of effects due to plastic relaxation, the small differences that were observed in erosion behavior support the suggestion that erosion at temperatures of up to 1000 °C is primarily a brittle process and that plastic relaxation plays only a minor role in establishing the erosion rate.

Acknowledgment

The authors gratefully acknowledge the support of the Office of Naval Research, Metallurgy and Ceramics Program.

Table 1: Properties of Target Materials Used in Erosion Study

Material	Young's Modulus (GPa)	Hardness (GPa)	Toughness, K_c ($MPa^{-m^{1/2}}$)	Microstructure
Hot-pressed silicon nitride	317 (a)	19.9 (m)	5.0 (f)	Fully dense ~ 1 μm grain size
Hot-pressed silicon carbide	466 (b)	29.4 (m)	4.0 (g)	Fully dense ~ 1-2 μm grain size
Hot-pressed aluminum oxide	425 (c)	22.0 (m)	4.0 (h)	Fully dense ~ 3-4 μm grain size
Sintered aluminum oxide	425 (c)	21.7 (m)	2.2 (i)	Fully dense ~ 30 μm grain size
Sapphire	425 (c)	21.7 (m)	2.2 (i)	Single crystal $\{10\bar{1}1\}$ plane
Silicon	168 (d)	20.6 (m)	0.7 (j)	Single crystal {112} plane
Silica glass	75 (e)	8.7 (m)	0.77 (k)	C7940
Soda-lime-silica glass	75 (e)	6.3 (m)	0.75 (k)	C0800
Magnesium oxide	330 (c)	8.0 (l)	2.6 (m)	Fully dense ~ 10-15 μm grain size

a[31]	d[34]	g[36]	j[25]	m[40]
b[32]	e[35]	h[37]	k[39]	
c[33]	f[26]	i[38]	l[22]	

Table 2: Velocity Exponents for Erosion Data: Normal Incidence

Material	Temperature 25 °C	500 °C	1000 °C
Magnesium oxide polycrystalline	2.2	--	--
Soda-lime-silica glass	2.5(.12)*	3.5(.20)	--
Vitreous silica	2.9	3.0	--
Sapphire	2.3(.10)	2.4(.25)	3.3(.03)
Sintered aluminum oxide, 30 μm	2.3(.003)	2.8(.09)	2.7(.15)
Hot-pressed aluminum oxide, 3-4 μm	2.3(.03)	2.1(.04)	2.3(.11)
Silicon	2.9(.03)	3.8	3.4
Hot-pressed silicon carbide	1.8(.16)	--	--
Hot-pressed silicon nitride	2.1(.08)	2.5(.03)	2.4(.20)

*The numbers in parentheses give the standard error for the value of the velocity exponent, which was determined by a linear regression analysis of the mean wear values given in table 1A. For exponents that were determined from only two wear values, no standard error is given.

Table 3: Velocity Exponents for Erosion Data: Normal Incidence

Target Material	Erosion Particles	Exponent	Reference
Soda-lime-silica glass	SiC, 120 grit	3.0	14
MgO (96.5 percent)	SiC, 120 grit	2.7	14
Al_2O_3 (99.5 percent)	SiC, 120 grit	2.6	14
Pyrex glass	Al_2O_3 30 μm 10 μm	2.2 2.7	15
Hot-pressed Si_3N_4	SiC 8 to 940 μm	4.0	16
Silicon	Al_2O_3 23 μm to 270 μm	3.4 to 2.6 depending on particle size	17
Reaction bonded SiC	Al_2O_3 130 μm 270 μm	2.3 2.0	18
Hot-pressed SiC	Al_2O_3 130 μm 270 μm	1.8 1.5	19

Table 4: Determination of the Exponents of Equations 8 and 8a by a Multivariable Regression Analysis, Room Temperature Data

Equation 8

Exponent	Regression Coefficient	Standard Error of Coefficient	Computed t
a	- 0.932	0.110	- 8.44
b	1.384	0.093	14.92

Intercept, ℓn A	- 11.40
Multiple correlation	0.971
r-squared	0.942
Standard error of estimate	0.415

Equation 8a

Exponent	Regression Coefficient	Standard Error of Coefficient	Computed t
a	- 0.905	0.106	- 8.56
b	1.312	0.096	13.66
c	- 0.669	0.364	- 1.84

Intercept, ℓn A	- 9.84
Multiple correlation	0.975
r-squared	0.950
Standard error of estimate	0.415

References

1. A. G. Evans, "Impact Damage Mechanics: Solid Projectiles," pp. 1-67 in Treatise on Materials Science and Technology, Vol. 16, Erosion, Carolyn M. Preece, ed., Academic Press, New York (1979).

2. A. W. Ruff and S. M. Wiederhorn, "Erosion by Solid Particle Impact," pp. 69-126 in Ref. 1.

3. B. J. Hockey and B. R. Lawn, "Electron Microscopic Observations of Microcracking about Indentations in Aluminum Oxide and Silicon Carbide," J. Mat. Sci. 10, 1275 (1975).

4. B. J. Hockey, S. M. Wiederhorn, and H. Johnson, "Erosion of Brittle Materials by Solid Particle Impact," pp. 379-402 in Fracture Mechanics of Ceramics, Vol. 3, Flaws and Testing, R. C. Bradt, D. P. H. Hasselman, and F. F. Lange, eds., Plenum Press (1973).

5. B. J. Hockey and S. M. Wiederhorn, "Erosion of Ceramic Materials: The Role of Plastic Flow," pp.26-1 to 26-10 in Proceedings of the Fifth International Conference on Erosion by Liquid and Solid Impact, 3-6 Sept. 1979, published by Cavendish Laboratories, University of Cambridge.

6. B. R. Lawn, B. J. Hockey, and S. M. Wiederhorn, "Atomically Sharp Cracks in Brittle Solids: An Electron Microscopy Study," J. Mat. Sci. 15, 1207 (1980).

7. B. R. Lawn and D. B. Marshall, "Indentation Fracture and Strength Degradation in Ceramics," pp. 205-229 in Ref. 4.

8. A. G. Evans, M. E. Gulden, and M. E. Rosenblatt, "Impact Damage in Brittle Materials in the Elastic-Plastic Regime," Proc. R. Soc. London Ser. A 361, 343-365 (1978).

9. S. M. Wiederhorn and B. R. Lawn, "Strength Degradation of Glass Impacted with Sharp Particles, I." J. Am. Ceram. Soc. 62, 66-70 (1979).

10. M. E. Gulden, "Correlation of Experimental Erosion Data with Elastic-Plastic Impact Models," J. Am. Ceram. Soc. 64, C59-C60 (1981).

11. S. M. Wiederhorn and D. Ellis Roberts, "A Technique to Investigate High Temperature Erosion of Refractories," Bull. Am. Ceram. Soc. 55, 185 (1976).

12. A. W. Ruff and L. K. Ives, "Measurement of Solid Particle Velocity in Erosive Wear," Wear 35, 195-199 (1975).

13. R. J. Fields, Jr., B. J. Hockey, and S. M. Wiederhorn, to be published.

14. G. L. Sheldon and I. Finnie, "The Mechanism of Material Removal in the Erosive Cutting of Brittle Materials," J. Engr. for Ind., Trans. ASME, 88, 393-400 (1966).

15. G. A. Sargent, P. K. Mehrotra, and H. Conrad, "Multiple Particle Erosion of Pyrex Glass," pp. 77-100 in Erosion: Prevention and Useful Applications, ASTM STP 664, W. F. Adler, ed., American Society of Testing and Materials, Philadelphia, PA (1979).

16. M. E. Gulden, "Solid Particle Erosion of High Technology Ceramics (Si_3N_4, Glass-Bonded Al_2O_3 and MgF_2)," pp. 101-122, in Ref. 15.

17. R. O. Scattergood and J. L. Routbort, "Velocity and Size-Dependence of the Erosion Rate of Silicon," Wear 67, 227-232 (1981).

18. J. L. Routbort, R. O. Scattergood, and A. P. L. Turner, "The Erosion of Reaction Bonded SiC," Wear 59, 363-375 (1980).

19. J. L. Routbort and R. O. Scattergood, "Anomalous Solid-Particle Erosion Rate of Hot-Pressed Silicon Carbide," J. Am. Ceram. Soc. 63, 593-595 (1980).

20. P. W. Bridgman, "Dimensional Analysis," Yale University Press, 1922, 1931.

21. B. R. Lawn, A. G. Evans, and D. B. Marshall, "Elastic/Plastic Indentation Damage in Ceramics: The Median/Radial Crack System," J. Am. Ceram. Soc. 63, 574-81 (1980).

22. J. H. Westbrook, "The Temperature Dependence of Hardness of Some Common Oxides," Rev. Hautes Temper. et Réfract. t.3, 47-57 (1966).

23. A. G. Atkins, "High Temperature Hardness and Creep," pp. 223-240 in The Science of Hardness Testing and its Research Applications," J. H. Westbrook and H. Conrad, eds., American Society for Metals, Metals Park, Ohio (1973).

24. T. N. Loladge, G. V. Bokuchava, and G. E. Davidova, "Temperature Dependencies of the Microhardness of Common Abrasive Materials in the Range of 20 to 1300 °C," pp. 251-257 in Ref. 23.

25. C. St. John, "The Brittle-to-Ductile Transition in Pre-Cleaved Silicon Single Crystals," Phil. Mag. 32, 1193-1212 (1975).

26. A. G. Evans and S. M. Wiederhorn, "Crack Propagation and Failure Prediction in Silicon Nitride at Elevated Temperatures," J. Mat. Sci. 9, 373-395 (1974).

27. M. G. Mendiratta, J. Wimmer, and J. Bransky, "Dynamic K_{IC} and Dynamic Flexural Strength of HS-130 Si_3N_4," J. Mat. Sci. 12, 212-214 (1977).

28. S. T. Gonazy and D. L. Johnson, "Impact Fracture of Ceramics at High Temperature," pp. 495-506 in Ref. 4.

29. S. M. Wiederhorn and B. J. Hockey, "Hot Erosion of Glass," J. Noncrystalline Solids, 38 and 39, 433-438 (1980).

30. H. P. Kirchner and R. M. Gruver, "Localized Impact Damage in a Viscous Medium (Glass)," pp. 365-377 in Ref. 4.

31. M. L. Torté, R. A. Alliegro, D. W. Richerson, M. E. Washburn, and G. Q. Weaver, "Silicon Nitride and Silicon Carbide for High Temperature Engineering Applications," Proc. Brit. Ceram. Soc. 22, 125-146 (1973).

W. S. Coblenz, "Elastic Moduli of Boron-Doped Silicon Carbide," J. Am. Ceram. Soc. 58, 530-531 (1975).

33. J. F. Lynch, C. G. Ruderer, and W. H. Duckworth, "Engineering Properties of Selected Ceramic Materials," Am. Ceram. Soc., Columbus, OH (1966).

34. R. J. Jaccodine, "Surface Energy of Germanium and Silicon," J. Electrochem. Soc. 110, 524-527 (1963).

35. J. R. Hutchins, III, and R. V. Harrington, "Glass," pp. 533-604 in Kirk-Othmer Encyclopedia of Chemical Technology, A. Standen, ed., John Wiley and Sons, New York (1966).

36. J. L. Chermant, R. Moussa, and F. Osterstock, "Propriétés Thermomécaniques et Analyse Statistique de Matériaux SiC, Si_3N_4, SiAlON et SILCOMPS," Rev. Int. des Hautes Temp. et des Réfractaires, 18, 5-55 (1981).

37. L. M. Barker, "Short Rod K_{IC} Measurements of Al_2O_3," pp. 483-494 in Ref. 4.

38. S. M. Wiederhorn, B. J. Hockey, and D. E. Roberts, "Effect of Temperature on the Fracture of Sapphire," Phil. Mag. 28, 783-796 (1973).

39. S. M. Wiederhorn, "Fracture Surface Energy of Glass," J. Am. Ceram. Soc. 52, 99-105 (1969).

40. R. W. Rice, S. W. Freiman, and P. F. Becer, "Grain-Size Dependence of Fracture Energy in Ceramics: I, Experiment," J. Am. Ceram. Soc. 64, 345-350 (1981).

41. J. M. Kay and R. M. Nedderman, An Introduction to Fluid Mechanics and Heat Transfer, Third Edition, Cambridge University Press, Cambridge (1974).

42. O. L. Davies, Statistical Methods in Research and Production, Oliver and Boyd, London (1957).

Figure Captions

1. Schematic diagram of erosion equipment (after Wiederhorn and Roberts [11]).

2. Erosion of brittle materials at 25 °C, normal incidence impact, 150 μm SiC particles. For clarity the error was given in Table 1A have been left off the figure.

3. Erosion of brittle materials at 500 °C, normal incidence impact, 150 μm SiC particles. For clarity the error was given in Table 1A have been left off the figure.

4. Erosion of brittle materials at 1000 °C, normal incidence impact, 150 μm SiC particles. For clarity the error was given in Table 1A have been left off the figure.

5. Comparison of the erosion data with the theories given by (a) Eq. (4)[8] and (b) Eq. (5)[2]. The volume lost per particle impact was selected from figure 2 at a velocity of 63 m/s.

6. Single particle impact damage in ceramic materials, optical micrographs: (a) soda-lime-silica glass, 90 m/s; (b) sapphire, 90 m/s; (c) hot-pressed, silicon nitride, 90 m/s.

7. Single particle impact damage in ceramic materials, scanning electron micrographs: (a) soda-lime-silica glass, 54 m/s; (b) hot-pressed aluminum-oxide, 90 m/s; (c) hot-pressed silicon nitride, 90 m/s.

Appendix A

Dimensionless Erosion Equation

This Appendix is written for those readers who are unfamiliar with the technique of dimensional analysis. A concise description of the technique can be found in reference 41. The procedure outlined in this reference are followed here.

Starting with equation (6), we assume that the wear rate can be expressed as a power series expansion of the parameters v_o, R, ρ, K_c, and H:

$$W = \sum_i \alpha_i \, (v_o^{a_i}, R^{b_i}, \rho^{c_i}, K_c^{d_i}, H^{e_i}) \qquad (1A)$$

α_i being a dimensionless coefficient for each term. The dimensions of each term in the expansion must equal the dimensions of w in order that equation (1A) to be dimensionally consistant. For the present study the dimensions of parameters given in equation (1A) are:

W	v_o	R	ρ	K_c	H
L^3	L/T	L	M/L^3	$M/T^2L^{0.5}$	M/T^2L

where L, T, and M represent the dimensions of length, time, and mass respectively.

When the dimensions are substituted for the parameters in equation (1A), each term in the expansion must have the following dimensional form:

$$L^3 = (L/T)^{a_i} \, L^{b_i} (M/L^3)^{c_i} (M/T^2L^{1/2})^{d_i} (M/T^2L)^{e_i} \qquad (2A)$$

Equating the exponents for each dimension we obtain the following set of equations

$$\begin{aligned} a_i + b_i - 3c_i - \tfrac{1}{2}d_i - e_i - 3 &= 0 \\ -a_i - 2d_i - 2e_i &= 0 \\ c_i + d_i + e_i &= 0 \end{aligned} \tag{3A}$$

Thus, we have a set of three equations in five unknowns. If two of the unknowns are selected as independent variables, the other unknowns can be expressed in terms of these two variables. For example, if c_i and d_i were selected then the following equations are obtained for a_i, b_i, and e_i:

$$\begin{aligned} a_i &= -3 - 2c_i \\ b_i &= 3 - d_i/2 \\ e_i &= -c_i - d_i \end{aligned} \tag{4A}$$

If these are substituted into equation (1A), the following expression is obtained for the wear rate W:

$$W/R^3 = \sum_i \alpha_i \, (v^2\rho/H)^{c_i} \, (K_c^2/RH^2)^{d_i/2} \tag{5A}$$

Since the two theories developed to explain erosion are power functions of the variables given in equation (5A), only one term in the series need be retained in order to compare the dimensional analysis with the theoretical expressions given by equations (4A) and (5A). Hence, the following relation is obtained for the erosion rate:

$$W/R^3 = A \, (K_c^2/RH^2)^a \, (\rho v^2/H)^b \tag{6A}$$

where A is a dimensionless constant and the exponents of equation (5A) have been written as a and b. Equation (6A) is identical to equation (7) of the text. As is noted earlier, the undetermined constants a and b are evaluated by an empirical fit of erosion data.

Equation (6A) is not a unique dimensionless representation of the parameters that control erosion. For example, if b_i and c_i had been selected as the independent constants, then the following erosion equation would have been obtained

$$W(H/K_c)^6 = A'(v^2\rho/H)^c \ (RH^2/K_c^2)^b \qquad (7A)$$

Equations (6A) and (7A) can be shown to be equivalent by dividing both sides of the equation by $(RH^2/K_c^2)^3$. By systematically solving for all possible combinations of the exponents in equation (1A), five variants of equation (6A) were found. These could all be reduced to equation (6A) by judicial manipulation (multiplying or dividing) by the dimensionless parameters K_c^2/RH^2 and $\rho v^2/H$.

There is a certain arbitrariness in selecting one of the dimensionless equations for a comparison with the experimental data. We justify the selection of equation (6A) on the basis of its simple form and the ease with which the dimensionless variables K_c^2/RH^2 and $\rho v^2/H$ can be given physical interpretation. Furthermore, this arrangement of the variables in equation (6A) separates the variants used in the present study more effectively than the others, and permits us to compare the theoretical equations with the results of the dimensional analysis more readily. Regardless of which form of the dimensionless analysis is used, one can show that they are all equivalent, provided the error is minimized in the term containing the wear rate, i.e., W/R^3. The equivalence is demonstrated by using the basic equations for a multiple regression analysis.

Appendix B

Table 1B: Summary of Erosion Data

Material	Temperature	Particle Velocity (m/s)	Erosion Rate (mm^3)
H.P. Si_3N_4	25 °C	94	7.4×10^{-7} (0.8)*
		73	4.0×10^{-7} (0.6)
		37	9.9×10^{-8} (2.6)
	500 °C	125	1.8×10^{-6} (0.2)
		90	8.1×10^{-7} (2.0)
		54	2.2×10^{-7} (0.4)
	1000 °C	125	2.5×10^{-6} (0.2)
		90	9.9×10^{-7} (0.5)
		54	3.4×10^{-7} (0.5)
H.P. SiC	25 °C	94	7.2×10^{-7} (1.5)
		73	5.3×10^{-7} (0.2)
		37	1.4×10^{-7} (0.3)
H.P. Al_2O_3	25 °C	94	1.1×10^{-6} (0.2)
		73	6.0×10^{7} (0.6)
		37	1.3×10^{-7} (0.4)
	500 °C	125	2.5×10^{-6} (0.1)
		100	1.5×10^{-6} (0.1)
		54	4.1×10^{-7} (0.1)
	1000 °C	125	2.5×10^{-6} (0.1)
		81	8.7×10^{-7} (0.6)
		54	3.8×10^{-7} (0.4)
Sintered Al_2O_3	25 °C	90	3.2×10^{-6} (0.4)
		73	2.0×10^{-6} (0.1)
		37	4.3×10^{-7} (1.3)
	500 °C	125	9.1×10^{-6} (1.0)
		90	3.9×10^{-6} (1.1)
		54	8.8×10^{-7} (3.6)

Sintered Al_2O_3	1000 °C	125	6.7×10^{-6} (2.1)
		90	2.8×10^{-6} (0.7)
		81	1.8×10^{-6} (0.6)
		54	7.0×10^{-7} (2.5)
Sapphire	25 °C	94	4.6×10^{-6} (0.4)
		54	1.2×10^{-6} (0.1)
		37	5.5×10^{-7} (0.1)
	500 °C	125	9.1×10^{-6} (1.0)
		90	3.9×10^{-6} (1.1)
		54	8.8×10^{-7} (3.6)
	1000 °C	125	9.8×10^{-6} (0.7)
		94	3.8×10^{-6} (0.3)
		54	6.4×10^{-7} (0.6)
Silicon	25 °C	94	2.1×10^{-5} (0.1)
		54	4.1×10^{-6} (0.3)
		37	1.4×10^{-6} (0.1)
	500 °C	125	6.5×10^{-5} (0.7)
		54	2.6×10^{-6} (0.2)
	1000 °C	125	7.7×10^{-5} (1.0)
		54	4.6×10^{-6} (0.7)
Sintered MgO	25 °C	94	7.3×10^{-5} (0.7)
		37	9.8×10^{-6} (0.2)
Fused Silica	25 °C	94	2.3×10^{-5} (0.3)
		37	1.6×10^{-6} (0.2)
	500 °C	125	6.0×10^{-5} (0.5)
		54	4.7×10^{-6} (0.0)
Soda-lime-silica glass	25 °C	94	3.2×10^{-5} (0.7)
		73	1.7×10^{-5} (0.4)
		54	7.1×10^{-6} (0.7)
		37	3.2×10^{-6} (0.7)
	500 °C	125	4.4×10^{-5} (1.2)
		100	2.2×10^{-5} (0.6)
		73	8.3×10^{-6} (0.4)
		54	2.3×10^{-6} (0.5)

*The numbers in parentheses are the standard deviation of each fit. Two to ten erosion measurements were used to determine each erosion rate.

SECURITY CLASSIFICATION OF THIS PAGE (When Data Entered)

REPORT DOCUMENTATION PAGE		READ INSTRUCTIONS BEFORE COMPLETING FORM
1. REPORT NUMBER	2. GOVT ACCESSION NO. AD-A115	3. RECIPIENT'S CATALOG NUMBER 288
4. TITLE (and Subtitle) EFFECT OF CONTACT DAMAGE ON THE STRENGTH OF CERAMIC MATERIALS		5. TYPE OF REPORT & PERIOD COVERED Annual 1 Oct. 1980-30 Sept. 1981
		6. PERFORMING ORG. REPORT NUMBER
7. AUTHOR(s) S. M. Wiederhorn, B. J. Hockey, and J. S. Nadeau		8. CONTRACT OR GRANT NUMBER(s) N00014-81-F-0002
9. PERFORMING ORGANIZATION NAME AND ADDRESS National Bureau of Standards Fracture and Deformation Division Washington, D.C. 20234		10. PROGRAM ELEMENT, PROJECT, TASK AREA & WORK UNIT NUMBERS
11. CONTROLLING OFFICE NAME AND ADDRESS Office of Naval Research 800 North Quincy Street Arlington, VA 22217		12. REPORT DATE 30 September 1981
		13. NUMBER OF PAGES
14. MONITORING AGENCY NAME & ADDRESS(if different from Controlling Office)		15. SECURITY CLASS. (of this report) Unclassified
		15a. DECLASSIFICATION/DOWNGRADING SCHEDULE

16. DISTRIBUTION STATEMENT (of this Report)

17. DISTRIBUTION STATEMENT (of the abstract entered in Block 20, if different from Report)

18. SUPPLEMENTARY NOTES

19. KEY WORDS (Continue on reverse side if necessary and identify by block number)

Ceramics; erosion; friction; impact, strength; tribology; wear

20. ABSTRACT (Continue on reverse side if necessary and identify by block number)

The primary objective of this research is the development of a deeper understanding of the physical processes that result in contact damage between components of heat engines at elevated temperatures. Rates of mechanical junction formation will be measured, and the effect of these junctions on friction, crack formation, and strength degradation will be investigated. Major material parameters to be studied will include ceramic composition, microstructure, hardness, and fracture toughness. The data obtained will be

DD FORM 1 JAN 73 1473 EDITION OF 1 NOV 65 IS OBSOLETE
S/N 0102-LF-014-6601

SECURITY CLASSIFICATION OF THIS PAGE (When Data Entered)

20. Abstract (continued)

used for the assessment of theoretical treatments of strength degradation caused by sliding contact stresses. During the past year, equipment has been constructed to measure the adhesive and frictional forces that develop between ceramics at elevated temperatures. Some tests have been conducted on glasses to determine the temperatures at which the friction is enhanced as a result of adhesion at the contact interface. Studies indicate that the coefficient of friction increases precipitously at a temperature that is $\sim$ 200 °C below the fictive temperature, suggesting that at this temperature, glass is sufficiently movile for junctions to form at the glass interface.

In addition to this work on adhesion and friction, studies conducted in previous years on the erosion of ceramics at elevated temperatures have been summarized. Erosion data are compared with two theories that have been suggested to explain the erosive behavior of solids. A dimensional analysis is applied to the variables that are important to erosion, and a multivariant, linear regression analysis is used to fit the data to the dimensional analysis. The results of the linear regression analyses are compared with the two theories in order to evaluate the applicability of these theories to erosion. Although semi-quantitative agreement of the data with the theories is obtained, some discrepancies are apparent. In particular, the dependence of erosion rate on hardness and critical stress intensity factor is greater than predicted by either of the two theories. These discrepancies are attributed primarily to microstructural aspects of erosion that are not modeled by either of the theories.


DATE
ILME
8